

Electronic Supplementary Information

The effect of conjugation in macrocyclic ring on the photophysical properties of a series of thiaaceneporphyrinoids

Young Mo Sung,^a Bartosz Szymczko,^b Radomir Mysliborski,^b Marcin Stępień,^b Juwon Oh,^a Minjung Son,^a Lechosław Latoś-Grażyński,^{b,*} and Dongho Kim^{a,*}

^aDepartment of Chemistry, Yonsei University, Seoul 120-749, Korea, ^bDepartment of Chemistry, University of Wrocław, 14 F. Joliot-Curie Street, 50-383, Wrocław, Poland.

E-mail: dongho@yonsei.ac.kr, lechoslaw.latos-grazynski@chem.uni.wroc.pl

Contents

1. Experimental Details

Scheme S1. Synthesis of Apor

Table S1. Crystal data and structure refinement for compounds Apor and *m*-Bpor

2. Supporting Information

Figure S1. The optimized structures (bottom) of a series of thiaaceneporphyrinoids (The optimized structures were calculated based on their X-ray structures (Figure 2).)

Figure S2. Calculated energy diagrams and MO of *m*-Bpor

Figure S3. Calculated energy diagrams and MO of *p*-Bpor

Figure S4. Calculated energy diagrams and MO of Npor

Figure S5. Calculated energy diagrams and MO of Apor

Figure S6. fs-TA spectra (left) and decay profiles (right) of a series of thiabenziporphyrins in

toluene

Figure S7. The fluorescence decay profiles of *p*-Bpor (top) and Npor (bottom) in toluene

Figure S8. The optimized structures of Npor in the ground state (left) and excited state (right)

Figure S9. The calculated single point energy of a series of thiaaceneporphyrinoids changing with the torsional angles between the porphyrin frameworks and benzene moieties (Figure S1, The single point energy calculations were performed at B3LYP/6-31G (d,p) level by G09 program.)

Figure S10. The steady state results of a series of thiabenziporphyrins in paraffin oil (black line: absorption spectra, blue line: fluorescence spectra)

Figure S11. fs-TA spectra (left) and decay profiles (right) of a series of thiabenziporphyrins in paraffin oil

Figure S12. The fluorescence decay profiles of *p*-Bpor (top) and Npor (bottom) in paraffin oil

Figure S13. Spectral changes of a series of thiabenziporphyrins upon protonation in the absorption (left) and fluorescence (right) (red: neutral, blue: protonated form)

Figure S14. The fluorescence decay profiles of a series of thiabenziporphyrins at 77 K

Figure S15. fs-TA spectra (left) and decay profiles (right) of *m*-Bpor (top) and Apor (bottom)

Figure S16. The ACID plots of *m*-Bpor (isosurface valuce=0.05)

Figure S17. The ACID plots of *p*-Bpor (isosurface valuce=0.05)

Figure S18. The ACID plots of Npor (isosurface valuce=0.05)

Figure S19. The ACID plots of Apor (isosurface valuce=0.05)

Figure S20. The ACID plots of Apor (left: 60°, right: 80°, isosurface valuce=0.05)

Table S2. The photophysical properties of a series of thiabenziporphyrins

Figure S21. The ¹H NMR spectrum of *m*-Bpor

Figure S22. The ¹H NMR spectrum of *p*-Bpor

Figure S23. The ¹H NMR spectrum of Apor

Figure S24. The ¹³C NMR spectrum of *m*-Bpor

Figure S25. The ¹³C NMR spectrum of *p*-Bpor

Figure S26. The ¹³C NMR spectrum of Apor

Figure S27. The experimental and simulated HR-MS spectrum of *m*-Bpor

Figure S28. The HR-MS spectrum of *p*-Bpor

Figure S29. The HR-MS spectrum of Apor

Figure S30. The electronic absorption spectrum of *m*-Bpor

Figure S31. The electronic absorption spectrum of *p*-Bpor

Figure S32. The electronic absorption spectrum of Apor

Table S3. TD-DFT (B3LYP/6-31G(d,p)) calculated energies, oscillator strengths and compositions of the major electronic transitions of *m*-Bpor

Table S4. TD-DFT (B3LYP/6-31G(d,p)) calculated energies, oscillator strengths and compositions of the major electronic transitions of *p*-Bpor

Table S5. TD-DFT (B3LYP/6-31G(d,p)) calculated energies, oscillator strengths and compositions of the major electronic transitions of Npor

Table S6. TD-DFT (B3LYP/6-31G(d,p)) calculated energies, oscillator strengths and compositions of the major electronic transitions of Apor

1. Experimental Details

Temperature Dependent Experiments. For the temperature-dependent steady-state and time-resolved absorption and emission studies, a temperature-controlled liquid nitrogen cryostat (Oxford Instruments: Optistat DN) was used. The variable temperature femtosecond transient absorption experiments were conducted using a Janis VNF-100 cryostat with a Cryo-con 32B temperature controller. Temperatures were maintained to within ± 0.05 K and allowed to equilibrate for 30 minutes before spectroscopic measurements. The samples were degassed with Ar gas in order to exclude any effects from quenching reactions caused by oxygen. The results were controlled by comparison with measurements in a regular cuvette at room temperature.

Steady-state Absorption and Emission Measurements. Steady-state absorption spectra were obtained with an UV-VIS-NIR spectrometer (Varian, Cary5000) and steady-state fluorescence spectra were measured on a Hitachi model F-2500 fluorescence spectrophotometer and a Scinco model FS-2. For the observation of steady-state emission spectra in near-infrared (NIR) region, a photomultiplier tube (Hamamatsu, R5108), a lock-in amplifier (EG&G, 5210) combined with a chopper and a CW He-Cd laser (Melles Griot, Omnichrome 74) for the 442 nm excitation were used.

Time Correlated Single Photon Counting Measurements. Time-resolved fluorescence lifetime experiments were performed by the time-correlated single-photon-counting (TCSPC) technique. As an excitation light source, we used a Ti:sapphire laser (Mai Tai BB, Spectra-Physics) which provides a repetition rate of 800 kHz with ~ 100 fs pulses generated by a homemade pulse-picker. The output pulse of the laser was frequency-doubled by a 1 mm thickness of a second harmonic crystal (β -barium borate, BBO, CASIX). The fluorescence was collected by a microchannel plate photomultiplier (MCP-PMT, Hamamatsu, R3809U-51) with a thermoelectric cooler (Hamamatsu, C4878) connected to a TCSPC board (Becker&Hickel SPC-130). The overall instrumental response function was about 25 ps (the full width at half maximum (fwhm)). A vertically polarized pump pulse by a Glan-laser polarizer was irradiated to samples, and a sheet polarizer, set at an angle complementary to the magic angle (54.7°), was placed in the fluorescence collection path to obtain polarization-independent fluorescence decays.

Femtosecond Transient Absorption Measurements. The femtosecond time-resolved transient absorption (fs-TA) spectrometer consisted of Optical Parametric Amplifiers (Palitra, Quantronix) pumped by a Ti:sapphire regenerative amplifier system (Integra-C, Quantronix) operating at 1 kHz repetition rate and an optical detection system. The generated OPA pulses had a pulse width of ~ 100 fs and an average power of 100 mW in the range 280-2700 nm which were used as pump pulses. White light continuum (WLC) probe pulses were generated using a sapphire window (3 mm of thickness) by focusing of small portion of the fundamental 800 nm pulses which was picked off by a quartz plate before entering to the OPA. The time delay between pump and probe beams was carefully controlled by making the pump beam

travel along a variable optical delay (ILS250, Newport). Intensities of the spectrally dispersed WLC probe pulses are monitored by a High Speed spectrometer (Ultrafast Systems). To obtain the time-resolved transient absorption difference signal (DA) at a specific time, the pump pulses were chopped at 500 Hz and absorption spectra intensities were saved alternately with or without pump pulse. Typically, 4000 pulses excite samples to obtain the fs-TA spectra at a particular delay time. The polarization angle between pump and probe beam was set at the magic angle (54.7°) using a Glan-laser polarizer with a half-wave retarder in order to prevent polarization-dependent signals. Cross-correlation fwhm in pump-probe experiments was less than 200 fs and chirp of WLC probe pulses was measured to be 800 fs in the 400-800 nm region. To minimize chirp, all reflection optics in the probe beam path and the 2 mm path length of quartz cell were used. After the fluorescence and fs-TA experiments, we carefully checked absorption spectra of all compounds to detect if there were artifacts due to degradation and photo-oxidation of samples. HPLC grade solvents were used in all steady-state and time-resolved spectroscopic studies. The three-dimensional data sets of ΔA versus time and wavelength were subjected to singular value decomposition and global fitting to obtain the kinetic time constants and their associated spectra using Surface Xplorer software (Ultrafast Systems).

Computational Methods. Quantum mechanical calculations were performed with the Gaussian 09 program suite.¹ All calculations were carried out by the density functional theory (DFT) method with Becke's three-parameter hybrid exchange functionals and the Lee-Yang-Parr correlation functional (B3LYP), employing the 6-31G(d,p) basis set. The oscillator strength was calculated by performing a time dependent (TD)-DFT calculation.

NMR Spectroscopy. ¹H NMR spectra were recorded on a high-field spectrometers (¹H 600.15 MHz and 500.13 MHz), equipped with a broadband inverse gradient probeheads. Spectra were referenced to the residual solvent signal (chloroform-*d*, 7.24 ppm). Two-dimensional NMR spectra were recorded with 2048 data points in the *t*₂ domain and up to 1024 points in the *t*₁ domain, with a 1s recovery delay.

Mass Spectrometry. High resolution and Accurate Mass spectra were recorded on a Bruker microTOF-Q spectrometers using the electrospray technique.

X-Ray Crystallography. X-Ray quality crystals were prepared by slow diffusion of solution of **Thia *m*-Bpor** dissolved in dichloromethane into *n*-hexane or in the case of **Thia *p*-Apor** by slow diffusion of solution of **Thia-*p*-Apor** dissolved in dichloromethane into methanol. Data were collected at 100 K on a Xcalibur PX κ -geometry diffractometer, with Mo K α radiation ($\lambda=0.71073$ Å) and Xcalibur, Onyx diffractometer with Cu K α ($\lambda=1.54178$ Å). Data were corrected for Lorentz and polarization effects. Crystal data are compiled in Table S1. The structures were solved by direct methods with SHELXS-97² and refined by full matrix least-squares method by using SHELXL-97³ with anisotropic thermal parameters for the non-H atoms. Scattering factors were those incorporated in SHELXS-97.

Synthesis

Synthetic procedures and analytical data.

6,21-Diphenyl-11,16-di-p-tolyl-24-thia-m-benziporphyrin *m*-Bpor was synthesized according to the procedure described by Lash and co-workers.⁴

Yield: 50 mg (7.5%). **¹H NMR** (500 MHz, chloroform-*d*, 300 K): δ 7.46 – 7.42 (m, 6H), 7.40 – 7.38 (m, 4H), 7.33 (d, 4H, ³J = 7.9 Hz), 7.30 – 7.24 (m, 8H), 7.17 (s, 2H, 13,14-H), 7.07 (dd, 2H, ³J = 7.8 Hz, ⁴J = 1.7 Hz, 2,4-H), 6.63 (d, 2H, ³J = 4.7 Hz, pyrrole), 2.43 (s, 6H, 11,16-CH₃-Tol). **¹³C NMR** (126 MHz, chloroform-*d*, 300 K): δ 172.2, 154.8, 154.6, 147.4, 142.9, 139.7, 137.5, 136.8, 135.8, 135.4, 132.9, 132.6, 131.0, 129.8, 129.6, 128.9, 128.7, 128.5, 127.6, 112.7, 21.3. **HRMS** (ESI+): *m/z* 671.2514, calcd for C₄₈H₃₅N₂S⁺ 671.2515. **UV-Vis** (CH₂Cl₂, 298 K): λ_{max} (log ϵ) 321 (4.44), 341 (4.43), 413 (4.73), 653 (4.07).

5,20-Diphenyl-10,15-di-p-tolyl-24-thia-p-benziporphyrin *p*-Bpor was previously synthesized by Hung and co-workers.⁵ Herein we report on a different approach leading to *p*-Bpor. Analytical data are in agreement with those published for *p*-Bpor.

1,4-Bis(phenyl(2-pyrolyl)methyl)benzene⁶ (388 mg, 1 mmol) and 2,5-bis(tolylhydroxymethyl)tiophene⁷ (324 mg, 1 mmol), were added to dry dichloromethane (900 mL) under nitrogen. Boron trifluoride - etherate (100 μ L) was then added and the reaction mixture was protected from light and stirred for two hours. 2,3-Dichloro-5,6-dicyano-1,4-benzoquinone (DDQ; 681 mg, 3 mmol) was subsequently added and the reaction mixture was stirred for another half an hour. After that time solvent was evaporated under reduced pressure and the dark residue was subjected to chromatography (grade II alumina, dichloromethane). The desired product was eluted as a brown-green band. During the following chromatography (silica gel) after elution of dithiaporphyrin with dichloromethane, the desired product was eluted as green band with 5% methanol–dichloromethane solution. The crude product was recrystallized from dichloromethane – methanol. **Yield:** 89 mg (13%).

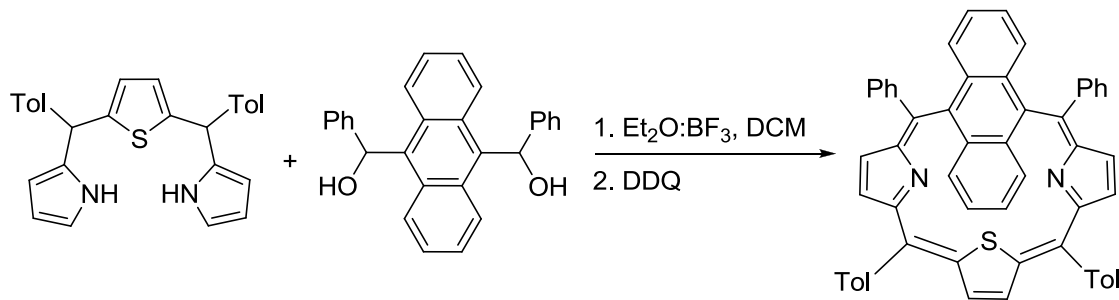
5,20-Diphenyl-10,15-di-p-tolyl-24-thia-1,4-naphthiporphyrin Npor was synthesized as described previously.⁸

5,20-Diphenyl-10,15-di-p-tolyl-24-thia-meso-anthriporphyrin Apor

2,5-Bis(tolyl(2-pyrrolyl)methyl)tiophene⁷ (1.59 g, 3.8 mmol) and 9,10-bis(phenylhydroxymethyl)anthracene⁹ (1.6 g, 4.0 mmol), were added to dry dichloromethane (900 mL) under nitrogen. Boron trifluoride - etherate (200 μ L) was then added and the reaction mixture was protected from light and stirred for two hours. 2,3-Dichloro-5,6-dicyano-1,4-benzoquinone (DDQ; 1.8 g, 7.6 mmol) was subsequently added and the reaction mixture was stirred for another half an hour. After that time solvent was evaporated under reduced pressure and the dark residue was subjected to chromatography (grade II alumina, dichloromethane). The desired product was eluted as a brown-green band. During the following chromatography (silica gel 70-230) after elution of dithiaporphyrin with dichloromethane, the desired product was eluted as a green band with 5% methanol –

dichloromethane solution. The crude product was recrystallized from dichloromethane – methanol. **Yield:** 170 mg (6%).

¹H NMR (600 MHz, chloroform-*d*, 300 K): δ 7.91 (d, 4H, ³J = 7.7 Hz, 5,20-*o*-Ph), 7.67 (d, 2H, ³J = 4.8 Hz, 7,18-H), 7.58 (AA'BB' spin system, 4H, 2¹,3¹, 21¹, 22¹-H), 7.50 (t, 4H, ³J = 7.7 Hz, 5,20-*m*-Ph), 7.46 (t, 2H, ³J = 7.7 Hz, 5,20-*p*-Ph), 7.17 (d, 4H, ³J = 8.0 Hz, 10,15-*o*-Tol), 7.13 (d, 4H, ³J = 8.0 Hz, 10,15-*m*-Tol), 7.11 (AA'BB' spin system, 4H, 2², 3², 21², 22²-H), 6.68 (s, 2H, 12,13-H), 6.68 (d partially covered with 12,13-H signal, 2H, 8,17-H), 2.38 (s, 6H, 10,15-CH₃-Tol). **¹³C NMR** (151 MHz, chloroform-*d*, 300 K): δ 168.1, 159.5, 153.4, 147.3, 140.6, 137.9, 137.1, 136.8, 136.1, 133.4, 131.9, 131.6, 130.9, 130.7, 129.3, 129.3, 128.9, 128.6, 126.8, 124.8, 21.2. **HRMS** (ESI+) *m/z* 771.2847, calcd for C₅₆H₃₉N₂S⁺ 771.2828. **UV–Vis** (CH₂Cl₂, 298 K): λ_{max} (log ϵ) 259 (4.92), 323 (4.30), 395 (4.73), 659 (4.21).



Scheme S1. Synthesis of Apor.

	Apor	<i>m</i>-Bpor
Empirical formula	C ₅₆ H ₃₈ N ₂ S, CH ₂ Cl ₂	C ₄₈ H ₃₄ N ₂ S, CH ₂ Cl ₂
Formula weight	855.87	755.76
Temperature	100 K	100 K
Wavelength	1.54178	0.71073
Crystal system	Triclinic	Monoclinic
Space group	P $\bar{1}$	P 2 ₁ /n
<i>a</i>	9.9886(2)	15.054(3)
<i>b</i>	13.3240(3)	16.560(3)
<i>c</i>	16.9907(4)	15.220(3)
α	91.846(2)	90
β	100.777(2)	96.87(3)
γ	102.672(2)	90
Volume	2160.93(8)	3767.0(13)
<i>Z</i>	2	4
Density (calculated)	1.315	1.333
Absorption coefficient	2.124	0.267
<i>F</i> (000)	892	1576
Crystal size	0.05x0.22x0.26	0.10x0.15x0.20
Theta range for data collection	2.65 $\leq \theta \leq$ 78.05	3.412 $\leq \theta \leq$ 28.479
Index ranges	-12 $\leq h \leq$ 12 -16 $\leq k \leq$ 16 -21 $\leq l \leq$ 17	-20 $\leq h \leq$ 18 -19 $\leq k \leq$ 21 -20 $\leq l \leq$ 20
Reflections collected	32471	8788
Independent reflections	9164	5885
Restraints	0	18
Parameters	561	515
Goodness-of-fit on <i>F</i> 2	1.075	1.007
Final R indices [<i>I</i> > 2 σ (<i>I</i>)]	0.0657	0.0723
R indices (all data)	0.0733	0.1284

Table S1. Crystal data and structure refinement for compounds Apor and *m*-Bpor.

Reference list

¹ Gaussian 09, Revision A.1, Frisch, M. J.; Trucks, G. W.; Schlegel, H. B.; Scuseria, G. E.; Robb, M. A.; Cheeseman, J. R.; Scalmani, G.; Barone, V.; Mennucci, B.; Petersson, G. A.; Nakatsuji, H.; Caricato, M.; Li, X.; Hratchian, H. P.; Izmaylov, A. F.; Bloino, J.; Zheng, G.; Sonnenberg, J. L.; Hada, M.; Ehara, M.; Toyota, K.; Fukuda, R.; Hasegawa, J.; Ishida, M.; Nakajima, T.; Honda, Y.; Kitao, O.; Nakai, H.; Vreven, T.; Montgomery, Jr., J. A.; Peralta, J. E.; Ogliaro, F.; Bearpark, M.; Heyd, J. J.; Brothers, E.; Kudin, K. N.; Staroverov, V. N.; Kobayashi, R.; Normand, J.; Raghavachari, K.; Rendell, A.; Burant, J. C.; Iyengar, S. S.; Tomasi, J.; Cossi, M.; Rega, N.; Millam, N. J.; Klene, M.; Knox, J. E.; Cross, J. B.; Bakken, V.; Adamo, C.; Jaramillo, J.; Gomperts, R.; Stratmann, R. E.; Yazyev, O.; Austin, A. J.; Cammi, R.; Pomelli, C.; Ochterski, J. W.; Martin, R. L.; Morokuma, K.; Zakrzewski, V. G.; Voth, G. A.; Salvador, P.; Dannenberg, J. J.; Dapprich, S.; Daniels, A. D.; Farkas, Ö.; Foresman, J. B.; Ortiz, J. V.; Cioslowski, J.; Fox, D. J. Gaussian, Inc., Wallingford CT, 2009.

² G. M. Sheldrick, *SHELXS97, Program for Crystal Structure Solution*; University of Göttingen: Göttingen, Germany, 1997.

³ G.M. Sheldrick, *SHELXL97, Program for Crystal Structure Refinement*; University of Göttingen: Göttingen, Germany, 1997.

⁴ T. D. Lash, A. M. Toney, K. M. Castans, G. M. Ferrence *J. Org. Chem.*, **2013**, 78, 9143-9152.

⁵ C. H. Hung, C. Y. Lin, P. Y. Lin, Y. J. Chen *Tetrahedron Lett.*, **2004**, 129-132.

⁶ M. Stępień, B. Szyszko, L. Latos-Grażyński *Org. Lett.* **2009**, 11, 3930-3933

⁷ A. Ulman, J. Manassen *J. Chem. Soc., Perkin Trans. 1*, **1979**, 1066-1069.

⁸ B. Szyszko, L. Latos-Grażyński *Organometallics* **2011**, 30, 4354-4363.

⁹ B. Szyszko, L. Latos-Grażyński, L. Szterenberg *Chem. Commun.* **2012**, 48, 5004-5006.

2. Supporting Information

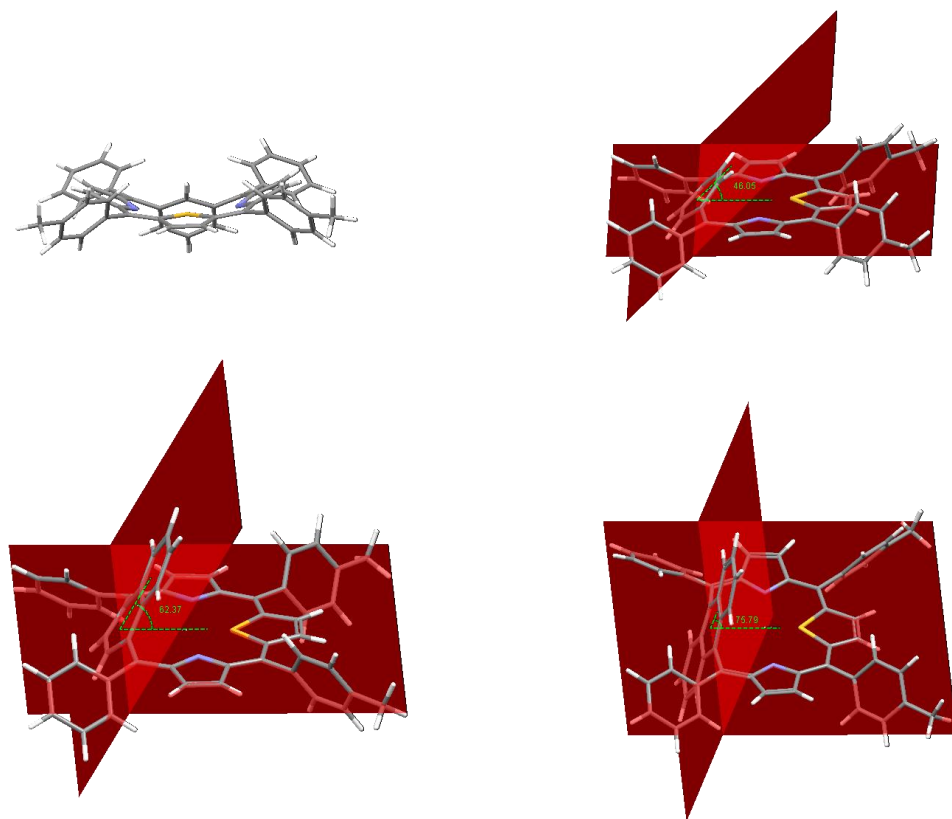


Figure S1. The optimized structures of a series of thiaaceneporphyrinoids (The optimized structures were calculated based on their X-ray structures (Figure 2).)

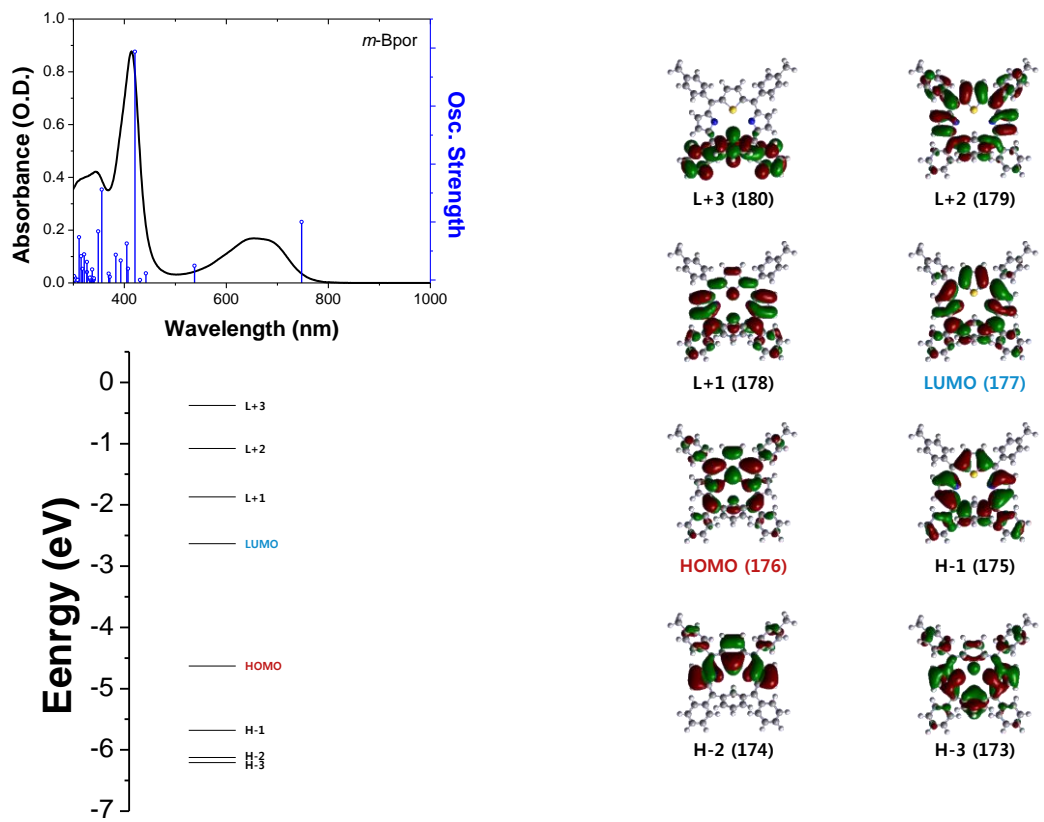


Figure S2. Calculated energy diagrams and MO of *m*-Bpor

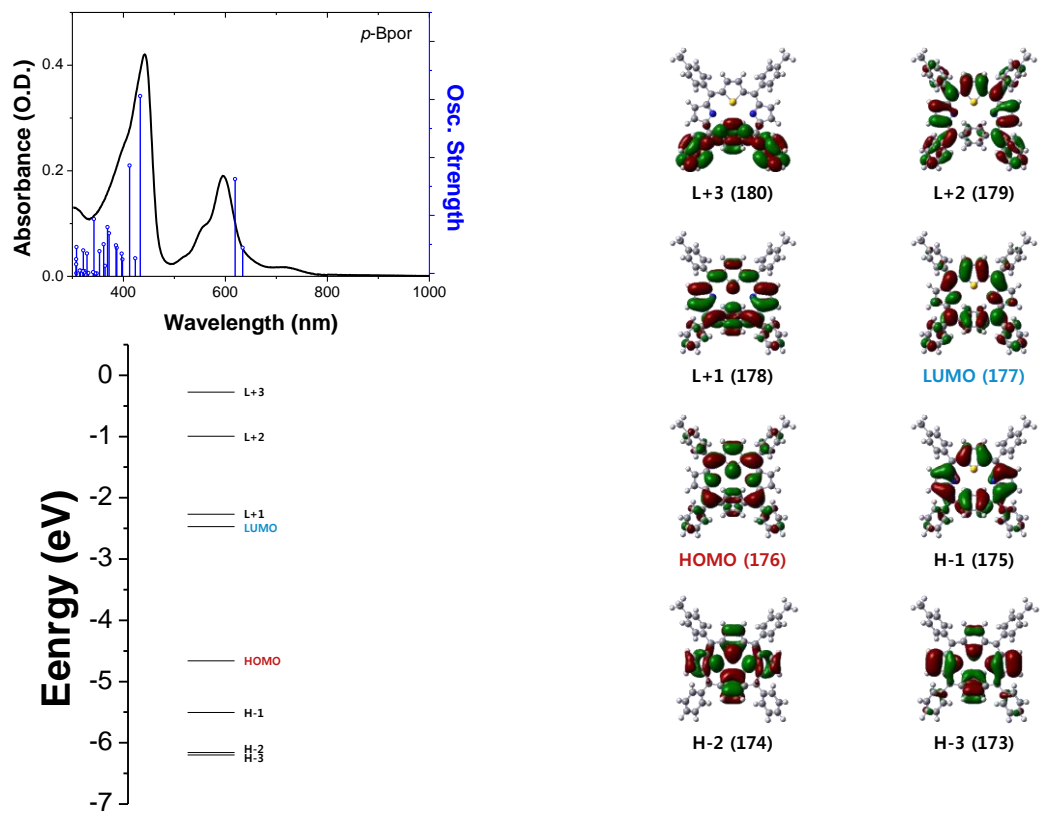


Figure S3. Calculated energy diagrams and MO of *p*-Bpor

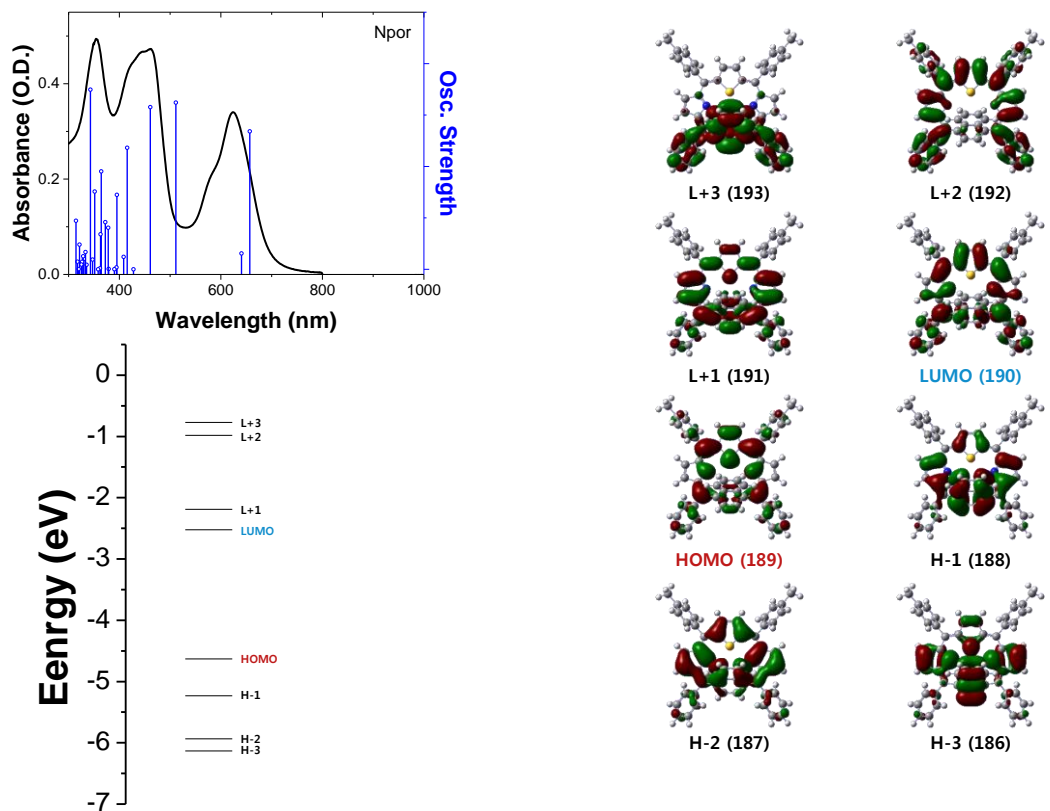


Figure S4. Calculated energy diagrams and MO of Npor

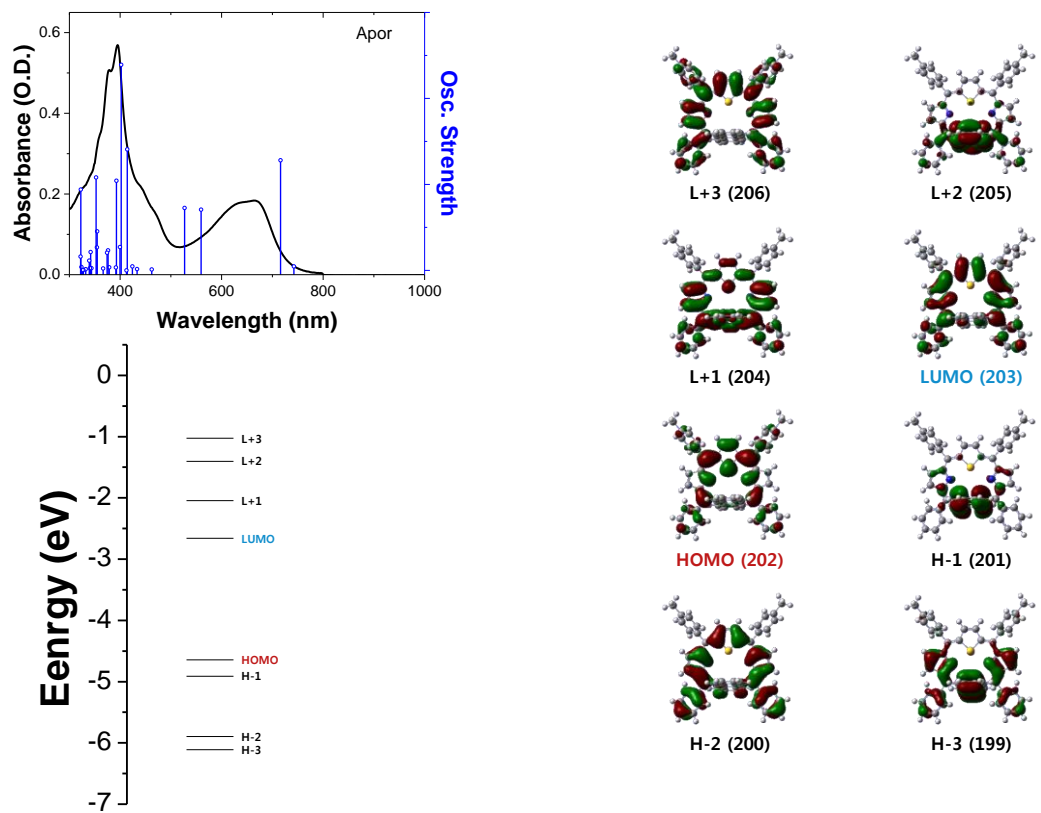


Figure S5. Calculated energy diagrams and MO of Apor

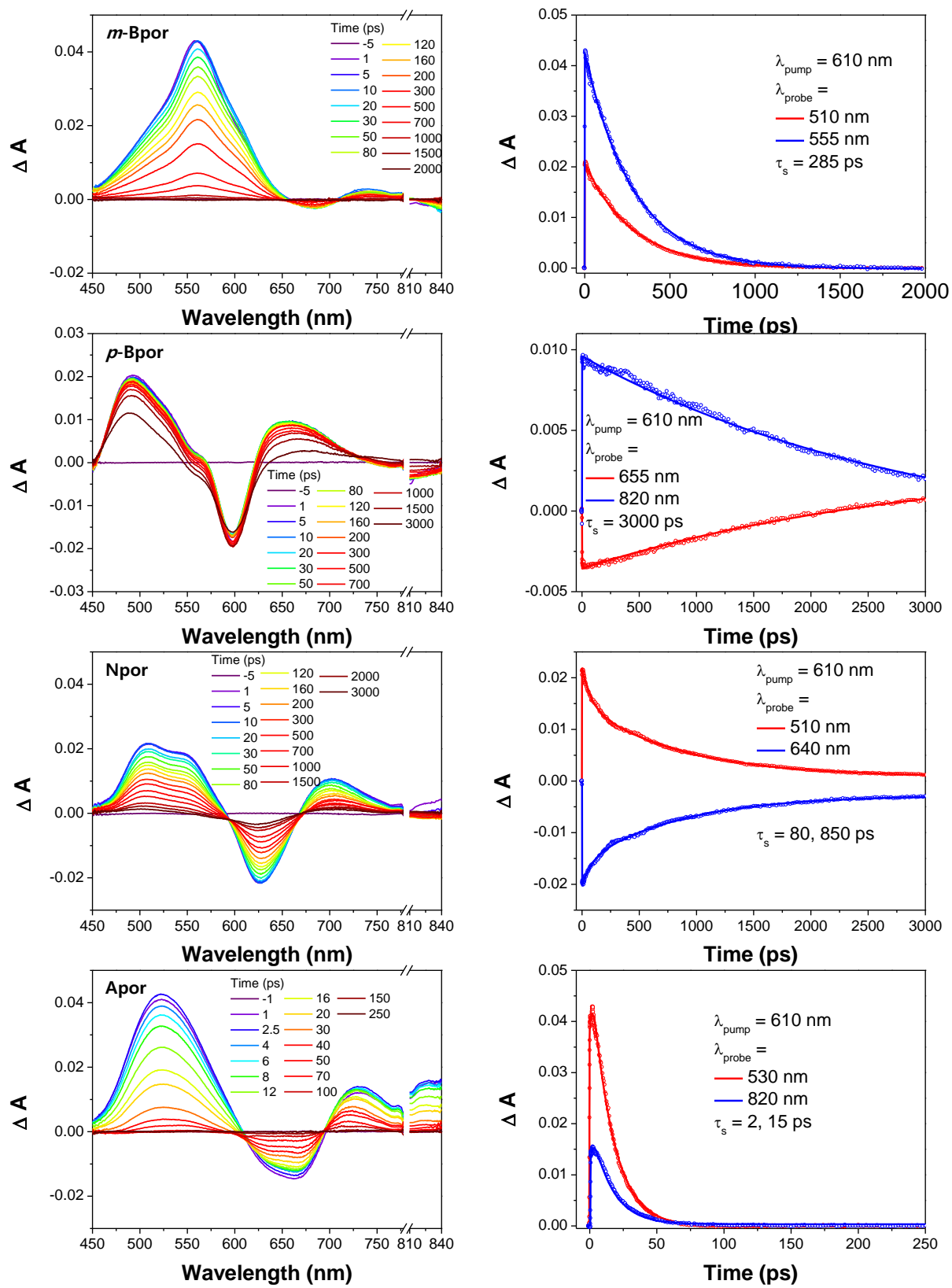


Figure S6. fs-TA spectra (left) and decay profiles (right) of a series of thiaaceneporphyrins in toluene

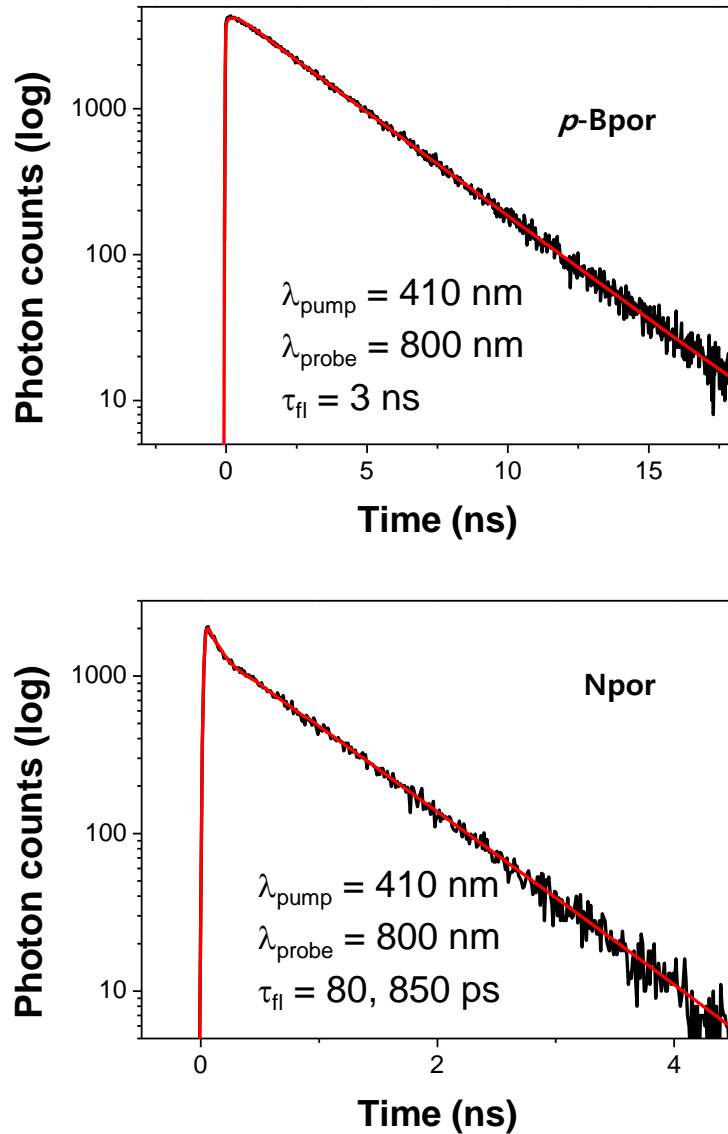


Figure S7. The fluorescence decay profiles of *p*-Bpor (top) and Npor (bottom) in toluene

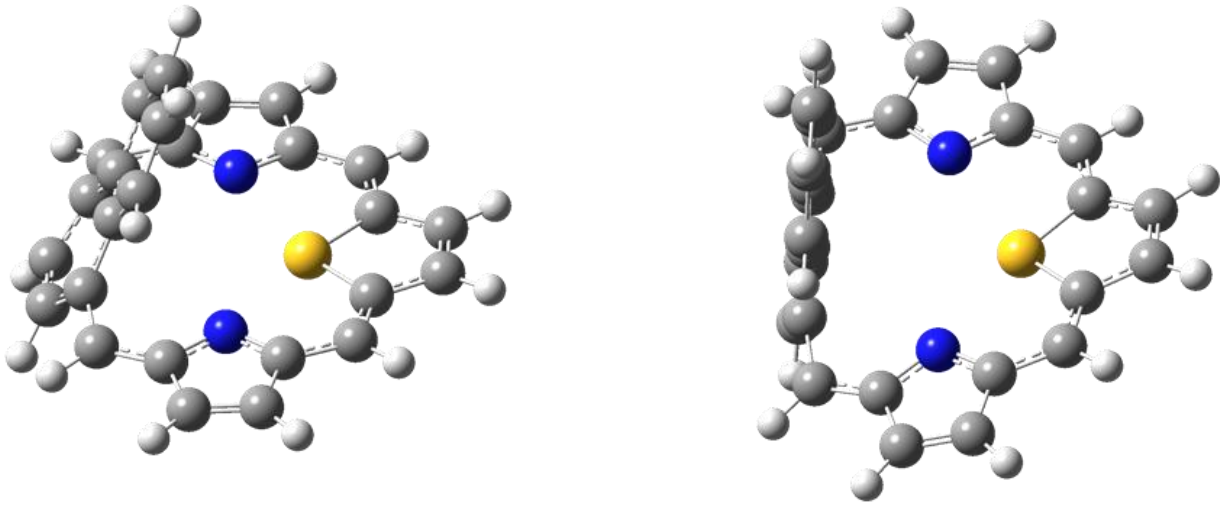


Figure S8. The optimized structures of Npor in the ground state (left) and excited state (right)

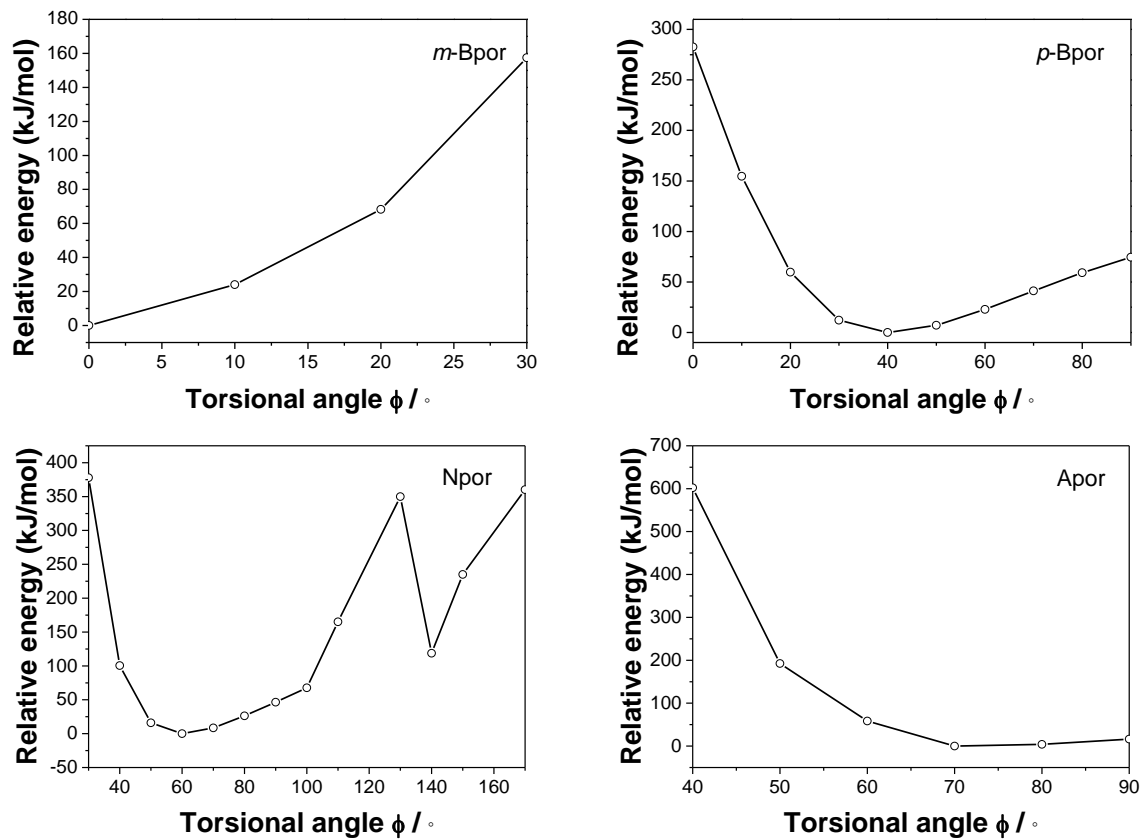


Figure S9. The calculated single point energy of a series of thiaaceneporphyrinoids changing with the torsional angles between the porphyrin frameworks and benzene moieties (Figure S1). The single point energy calculations were performed at B3LYP/6-31G (d,p) level by G09 program.

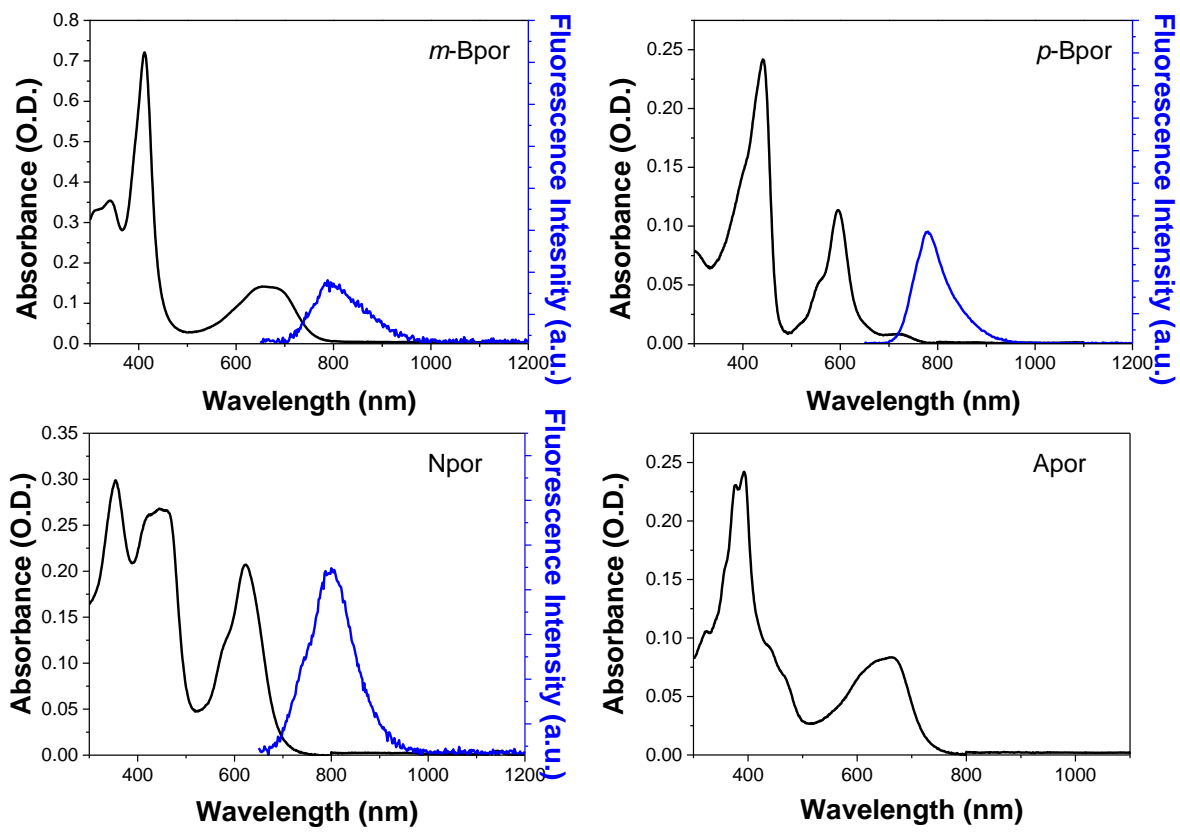


Figure S10. The steady state results of a series of thiabenziporphyrins in paraffin oil (black line: absorption spectra, blue line: fluorescence spectra)

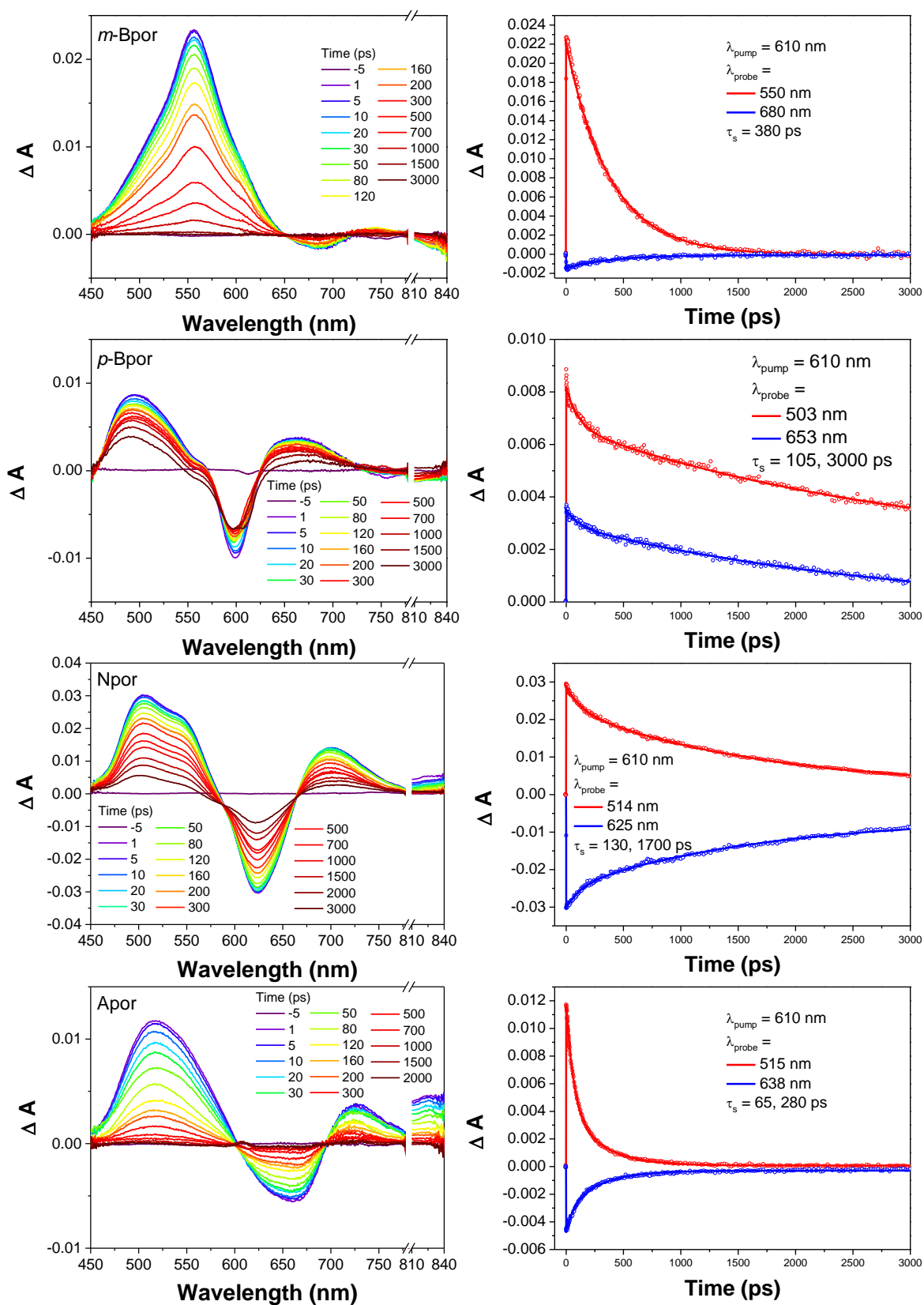


Figure S11. fs-TA spectra (left) and decay profiles (right) of a series of thiabenziporphyrins in paraffin oil

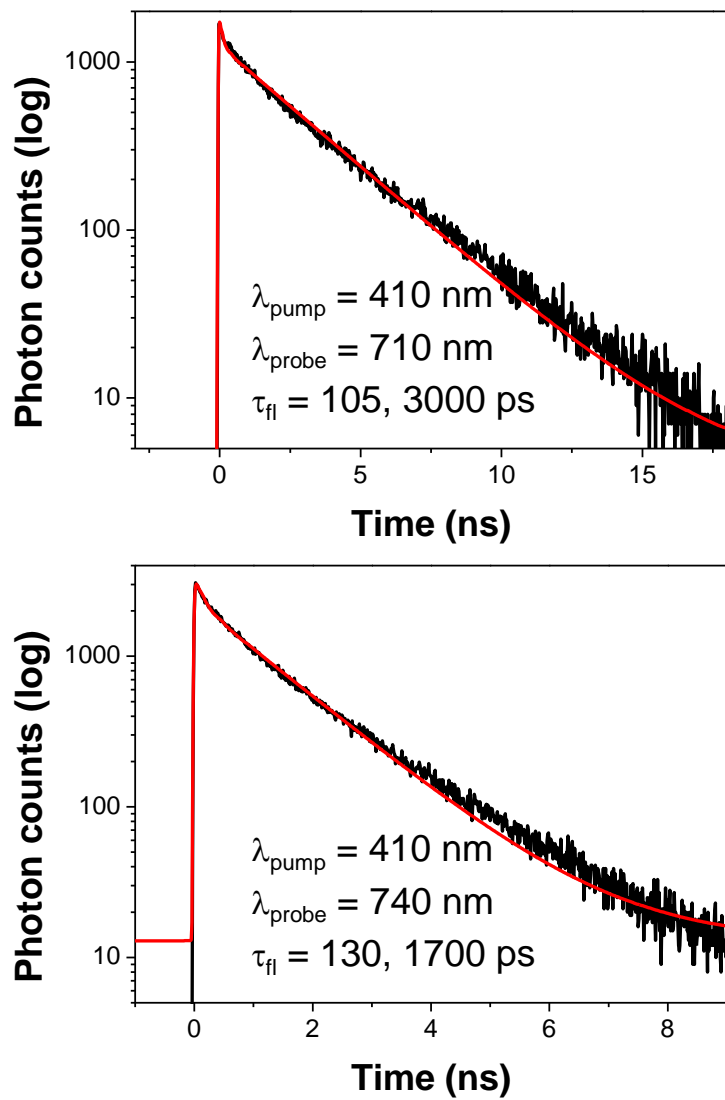


Figure S12. The fluorescence decay profiles of *p*-Bpor (top) and Npor (bottom) in paraffin oil

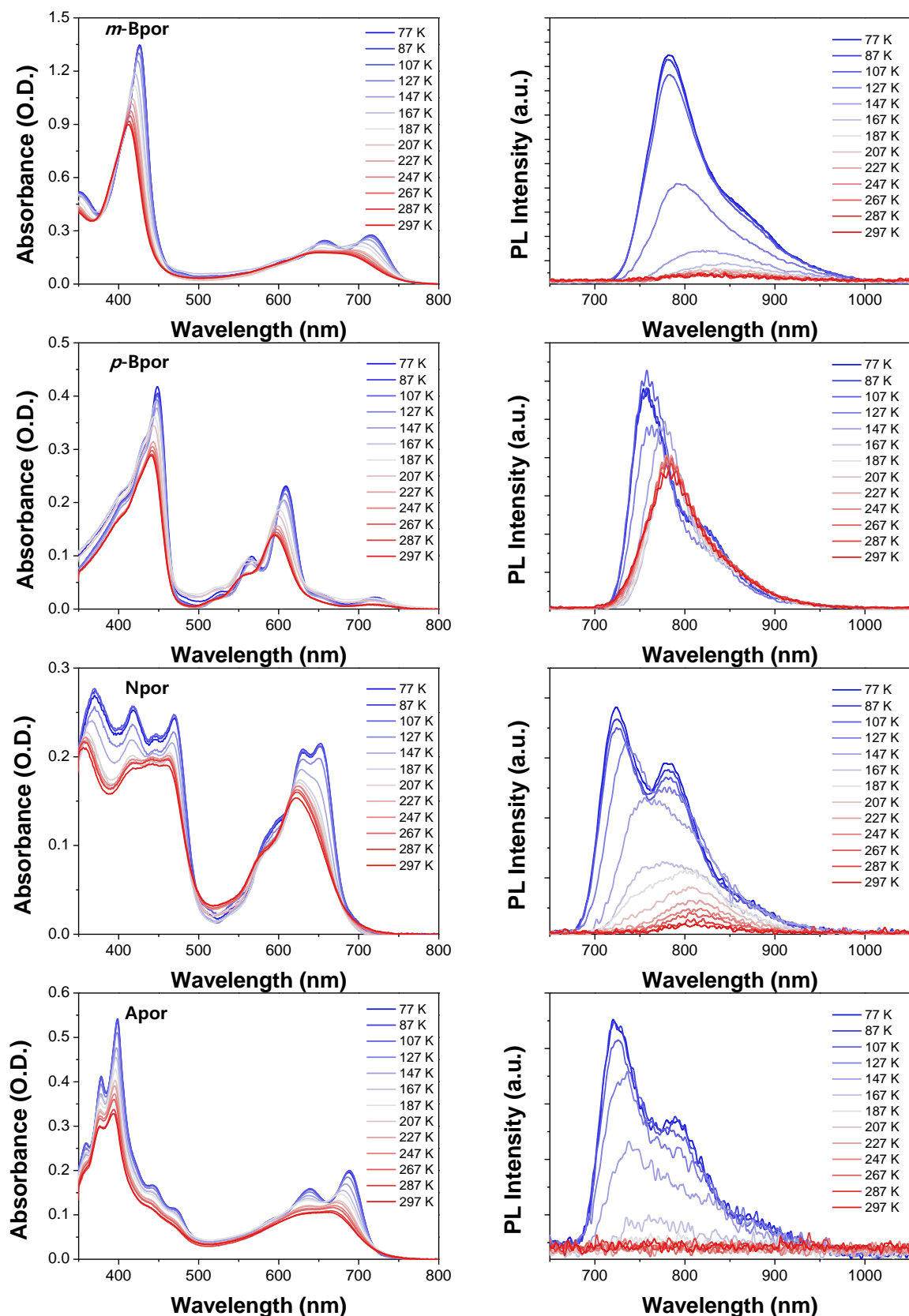


Figure S13. Spectral changes of a series of thiabenziporphyrins upon temperature change in the absorption (left) and fluorescence (right) (red: neutral, blue: protonated form)

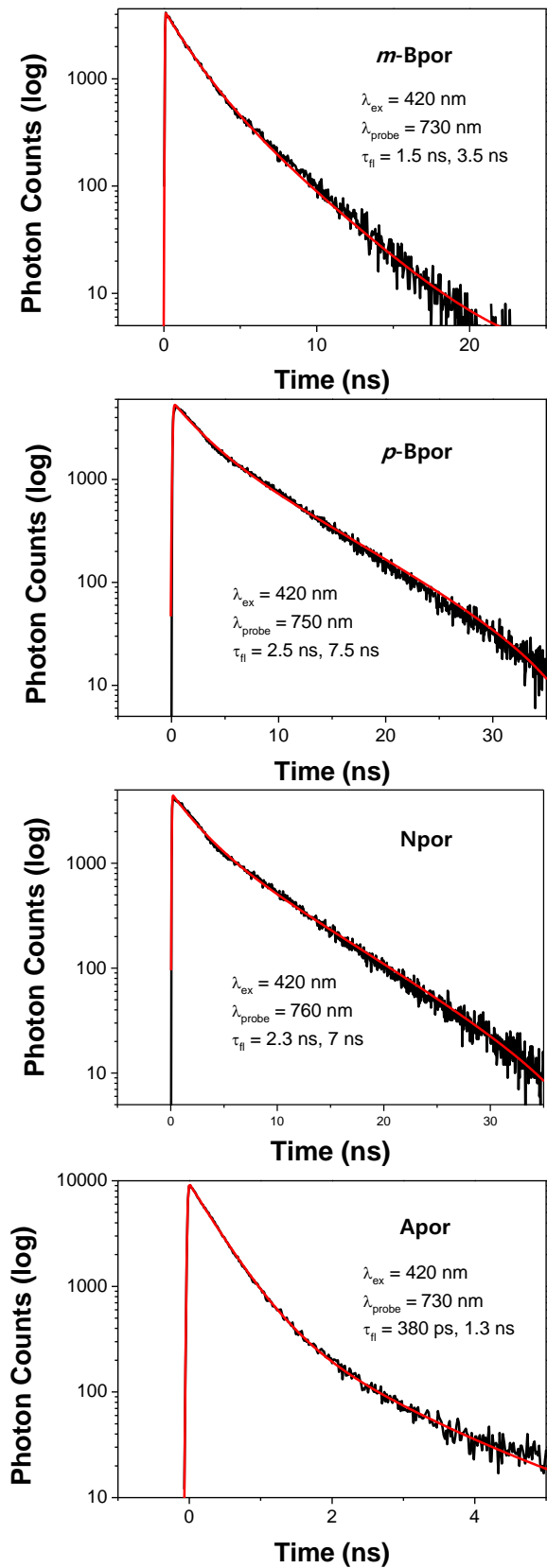


Figure S14. The fluorescence decay profiles of a series of thiabenziporphyrins at 77 K

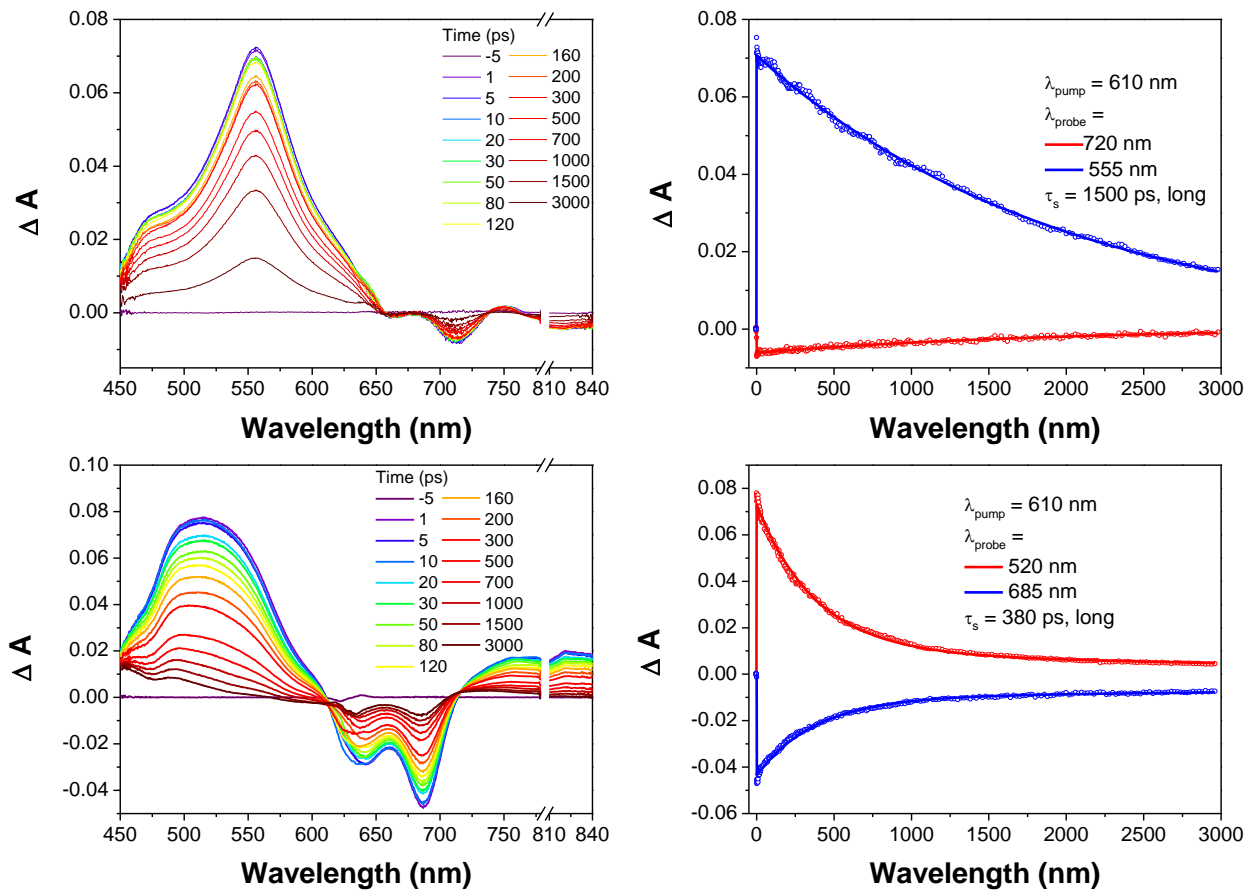


Figure S15. fs-TA spectra (left) and decay profiles (right) of *m*-Bpor (top) and Apor at 77 K (bottom)

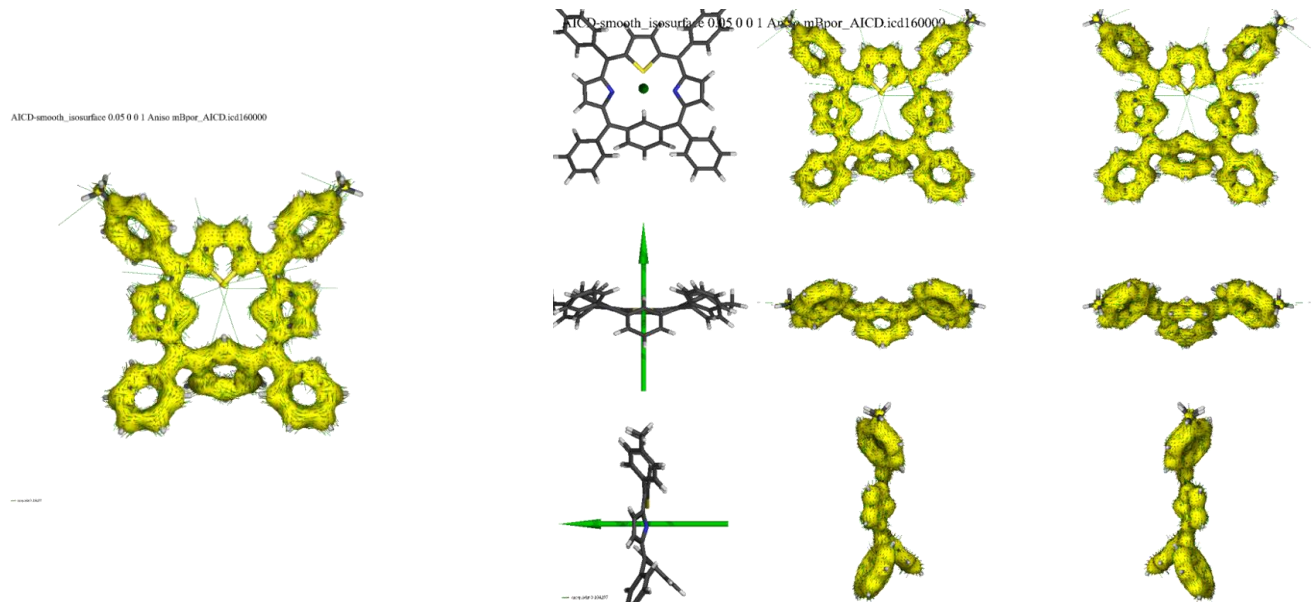


Figure S16. The ACID plots of *m*-Bpor with its optimized structure (isosurface valuce=0.05)

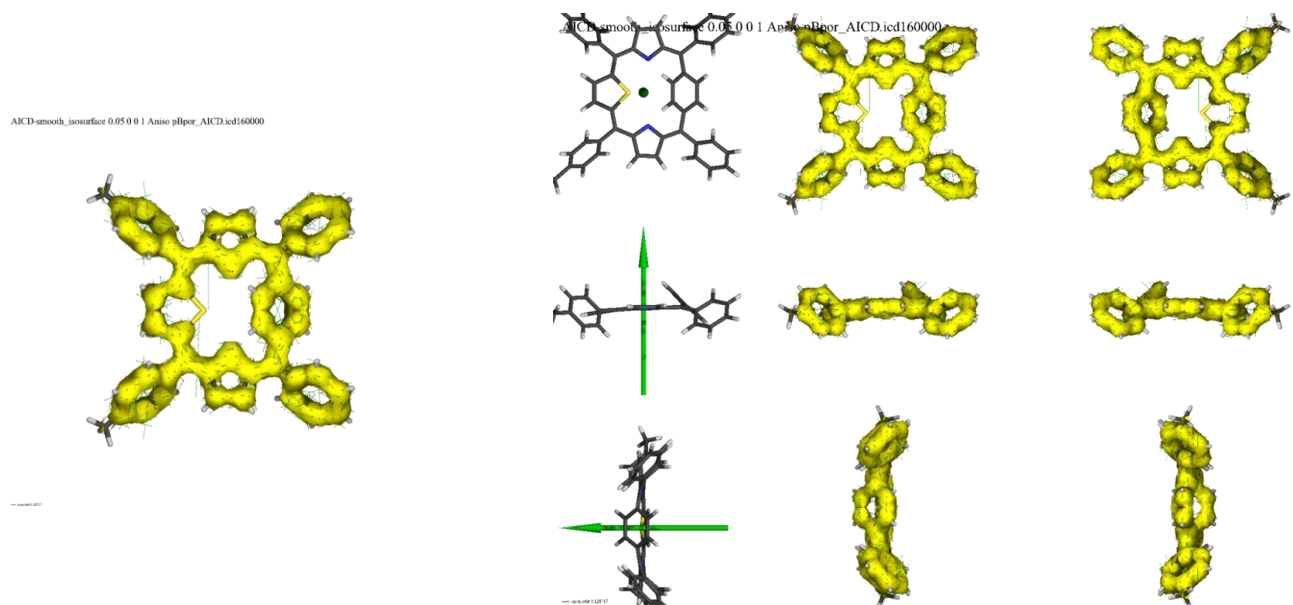


Figure S17. The ACID plots of *p*-Bpor with its optimized structure (isosurface valuce=0.05)

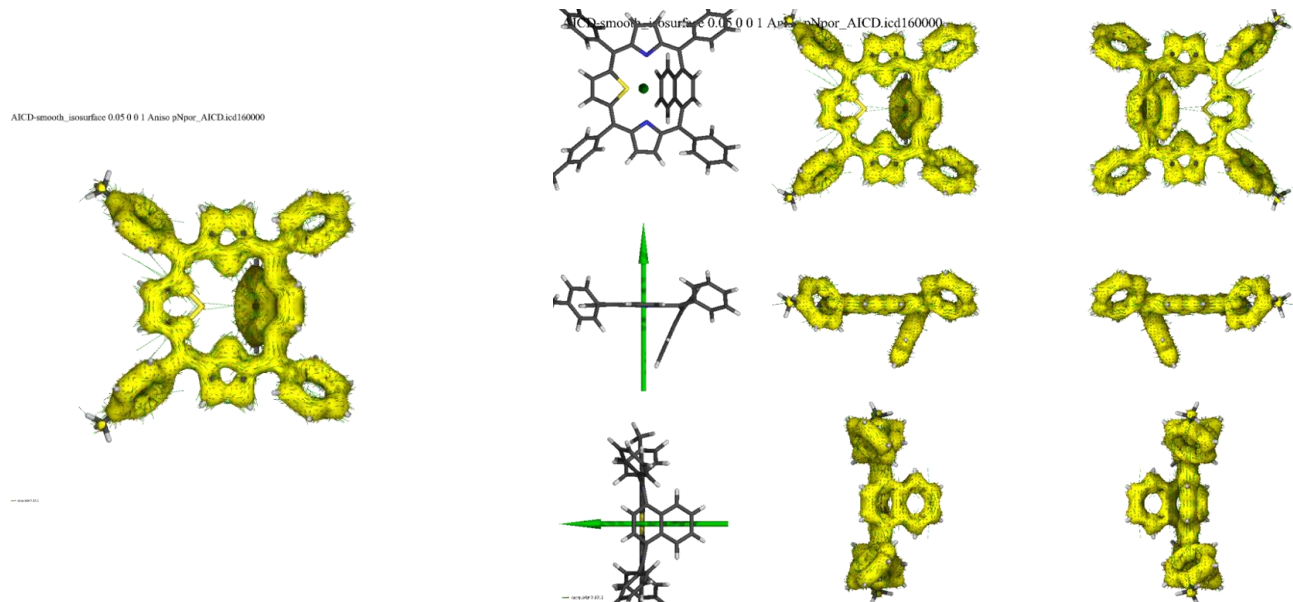


Figure S18. The ACID plots of Npor with its optimized structure (isosurface valuce=0.05)

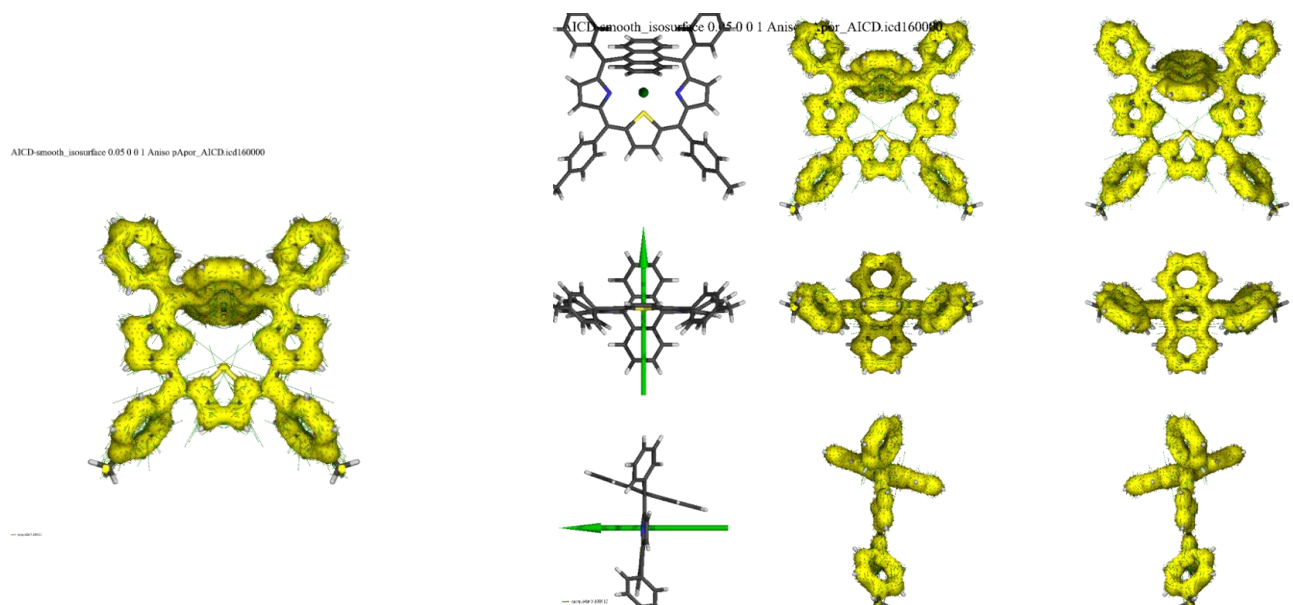


Figure S19. The ACID plots of Apor with its optimized structure (isosurface valuce=0.05)

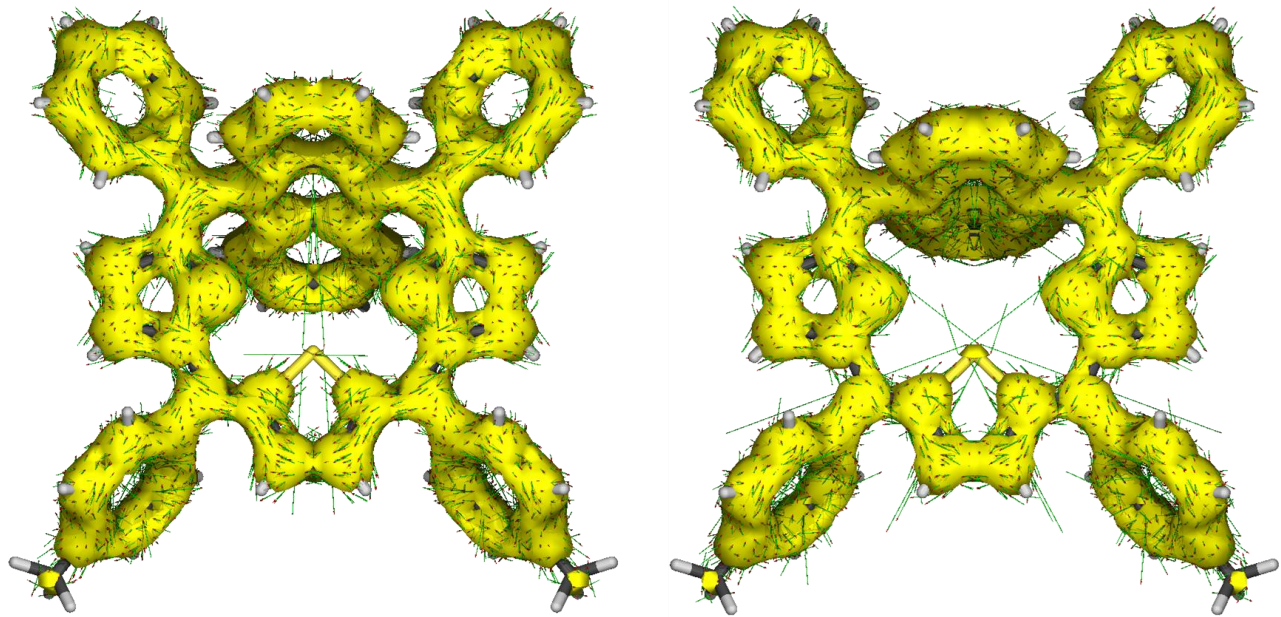


Figure S20. The ACID plots of Apor (left: 60° , right: 80° , isosurface value=0.05)

Table S2. The photophysical properties of a series of thiabenziporphyrins

		<i>m</i> -Bpor	<i>p</i> -Bpor	<i>p</i> -Npor	<i>p</i> -Apor
Δ Stokes shift (cm^{-1})	Toluene	2920	1220	3680	-
	Paraffin oil	2620	1160	3480	-
	77 K	1200	620	1550	720
τ_s (ps)	Toluene	285	3000	80, 850	2, 15
	Paraffin oil	380	105, 3000	130, 1700	65, 280
	77 K	1500, 3500	2500, 7500	2300, 7000	380, 1300

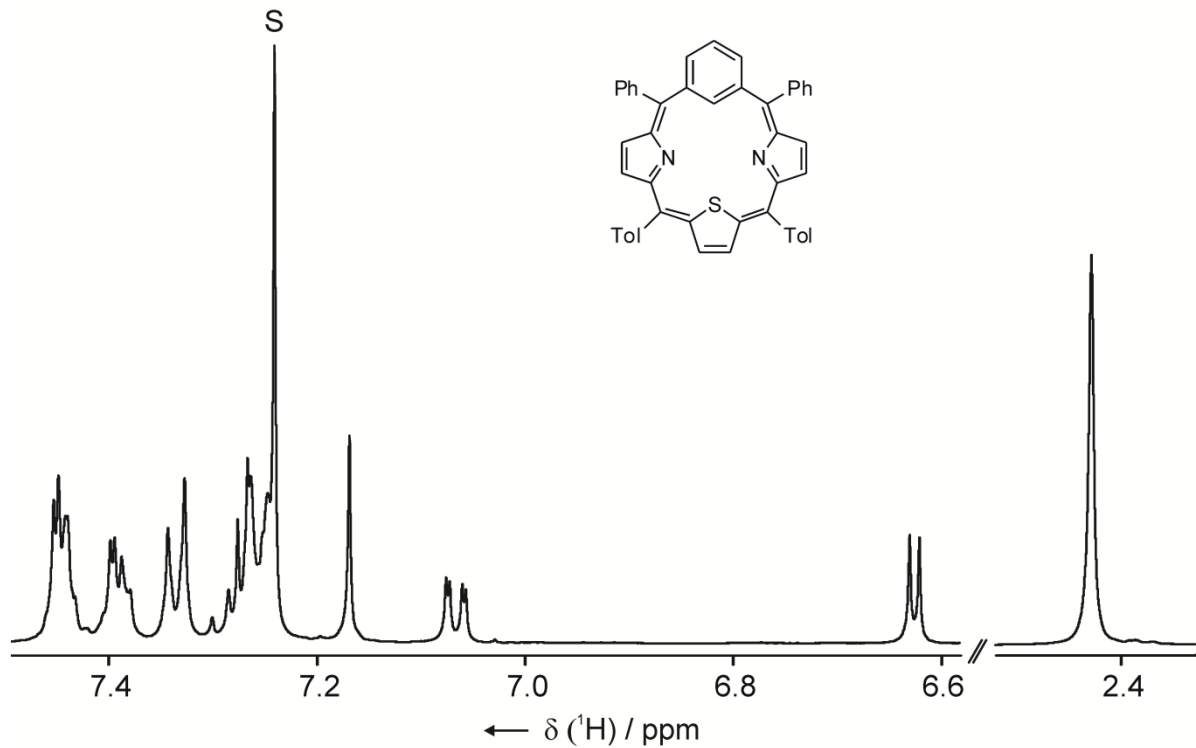


Figure S21. The ^1H NMR spectrum of *m*-Bpor (500 MHz, chloroform-*d*, 300 K)

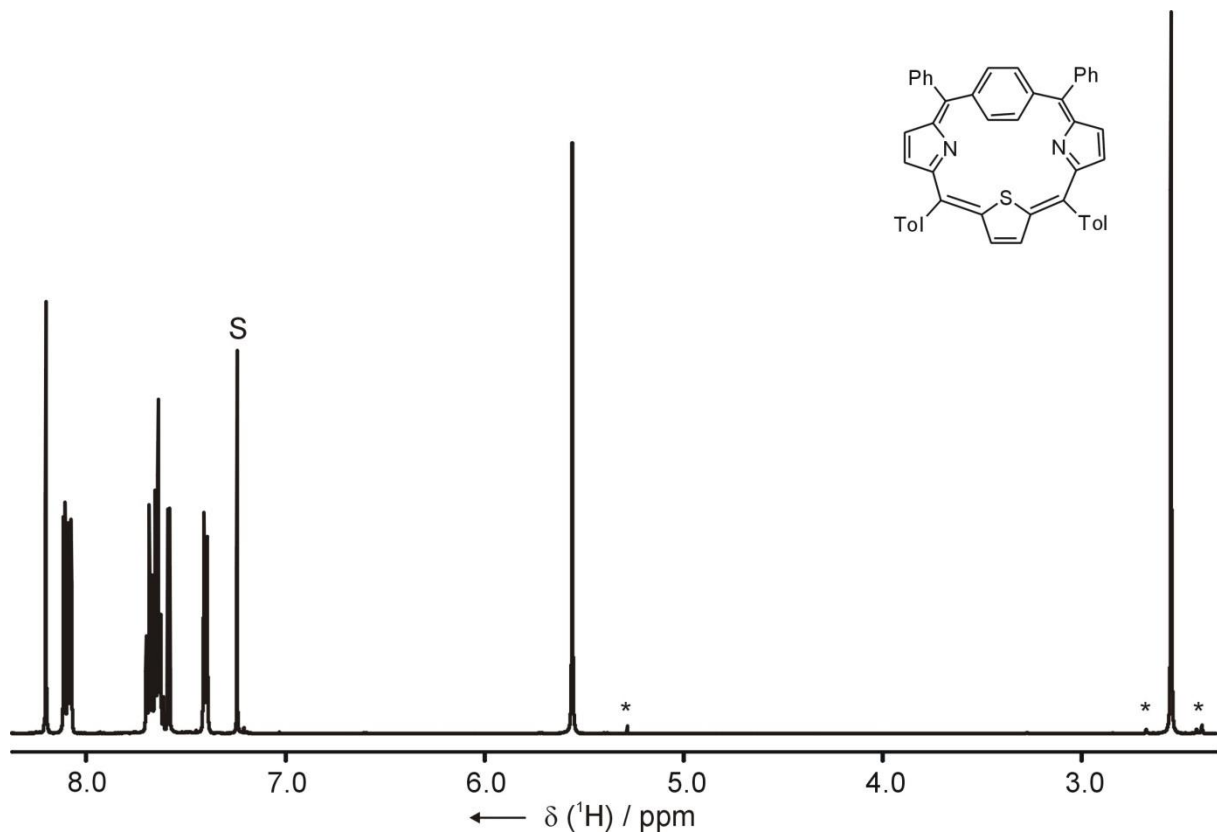


Figure S22. The ^1H NMR spectrum of *p*-Bpor (500 MHz, chloroform-*d*, 300 K)

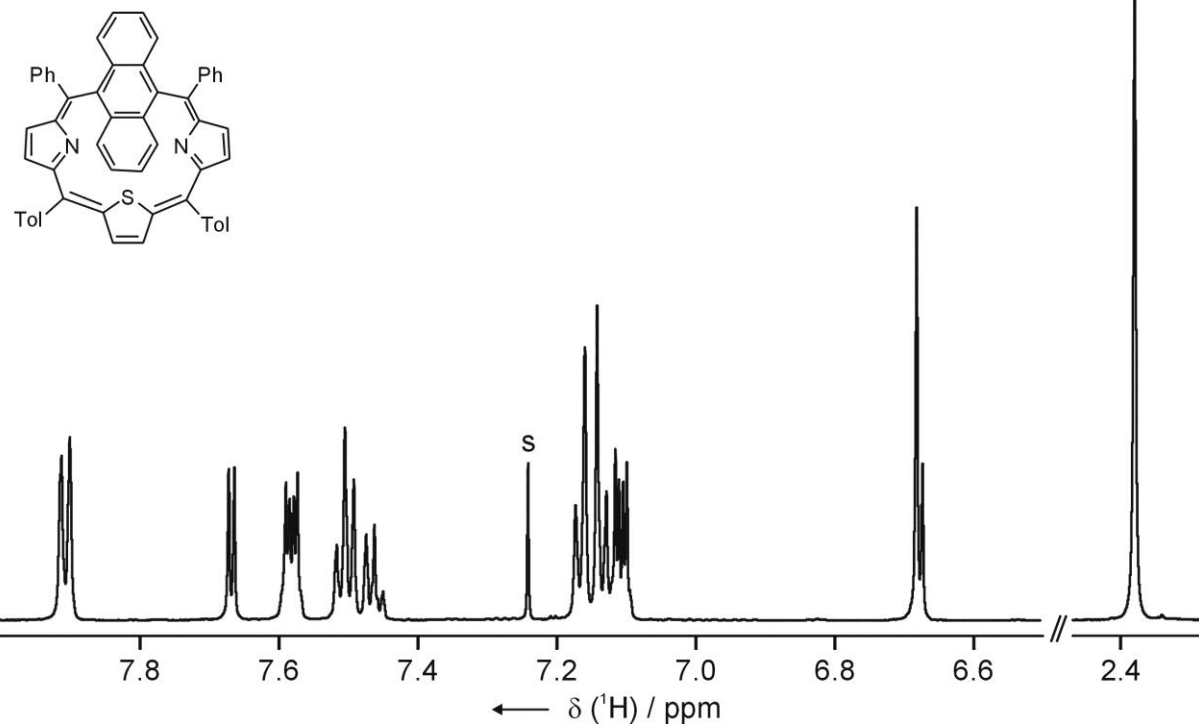


Figure S23. The ^1H NMR spectrum of Apor (600 MHz, chloroform-*d*, 300 K)

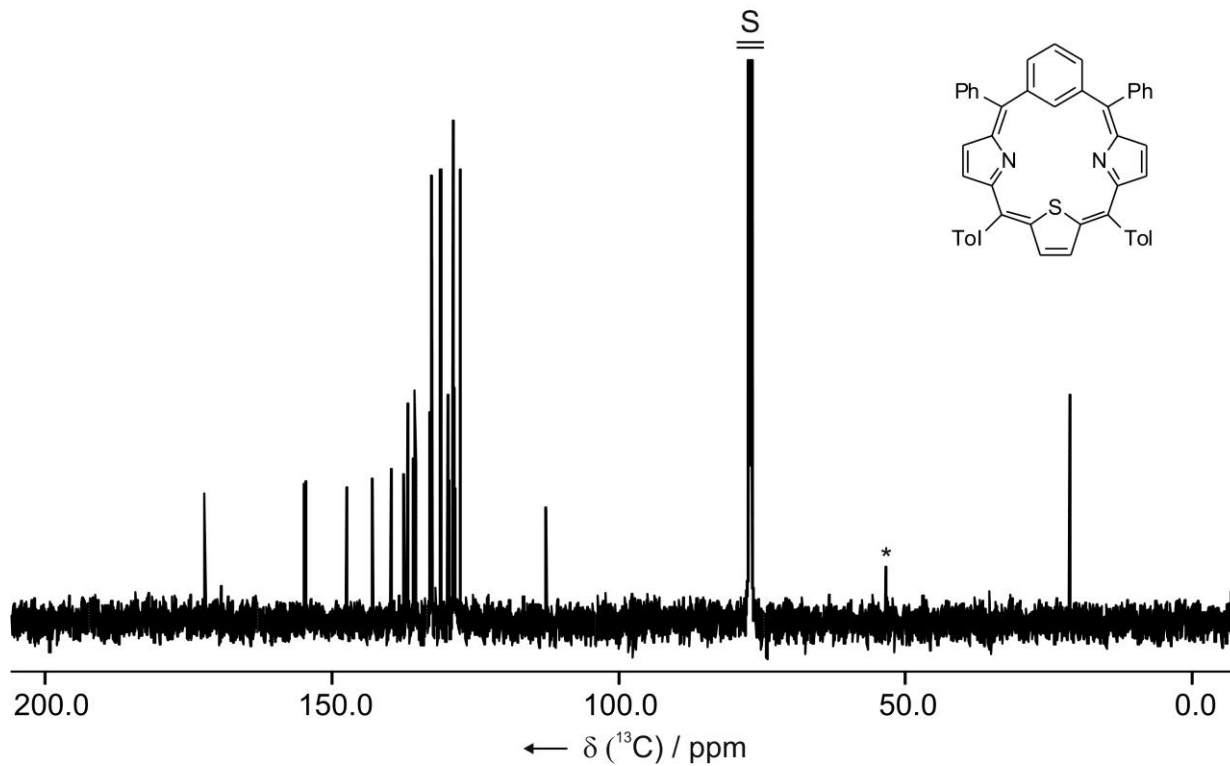


Figure S24. The ^{13}C NMR spectrum of *m*-Bpor (126 MHz, chloroform-*d*, 300 K)

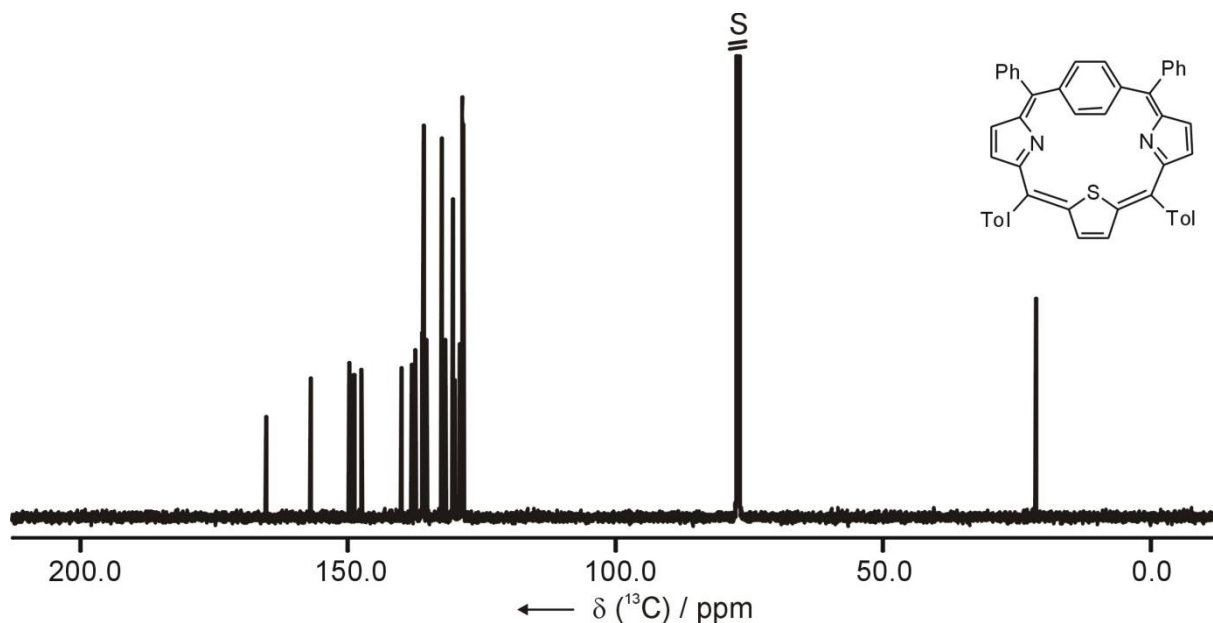


Figure S25. The ^{13}C NMR spectrum of *p*-Bpor (126 MHz, chloroform-*d*, 300 K)

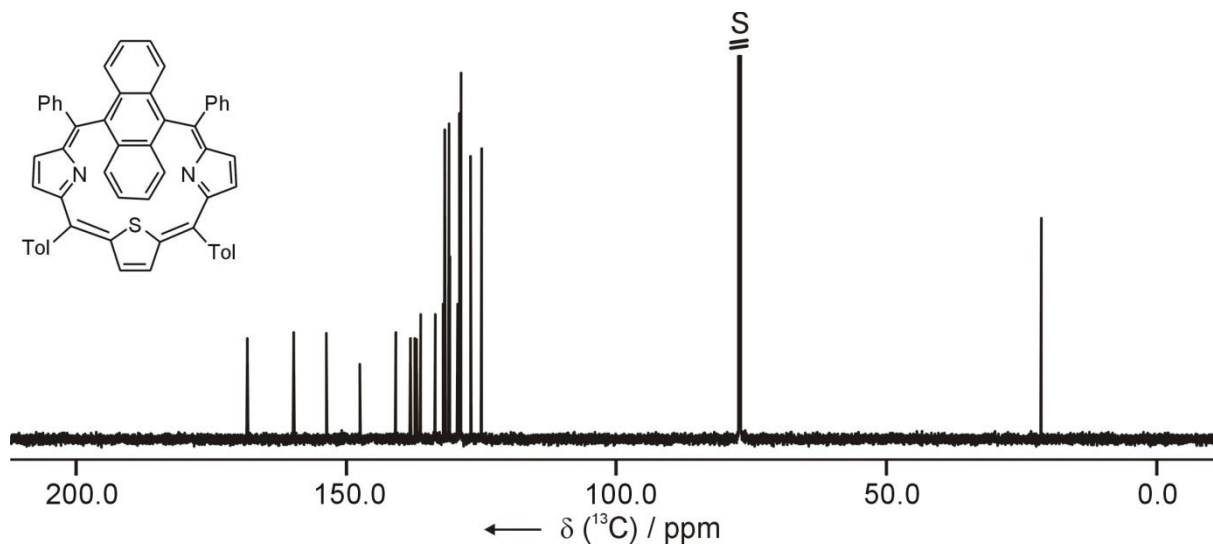


Figure S26. The ^{13}C NMR spectrum of Apor (151 MHz, chloroform-*d*, 300 K)

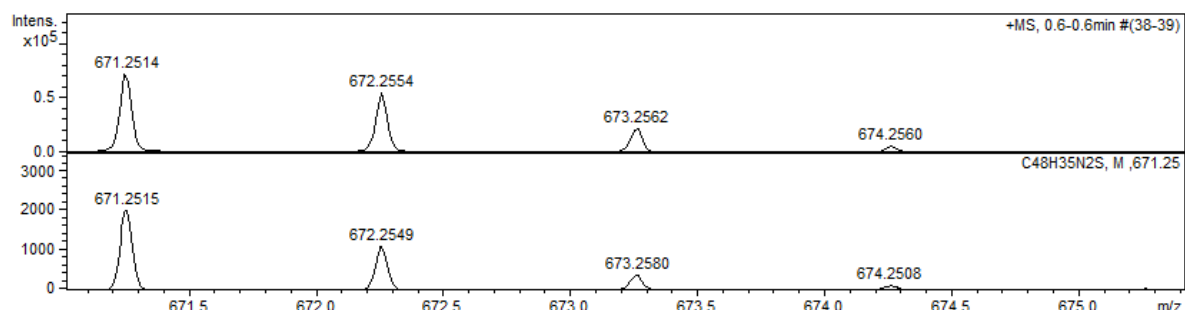


Figure S27. The experimental (top) and simulated (bottom) HR-MS spectrum of *m*-Bpor (ESI+, TOF).

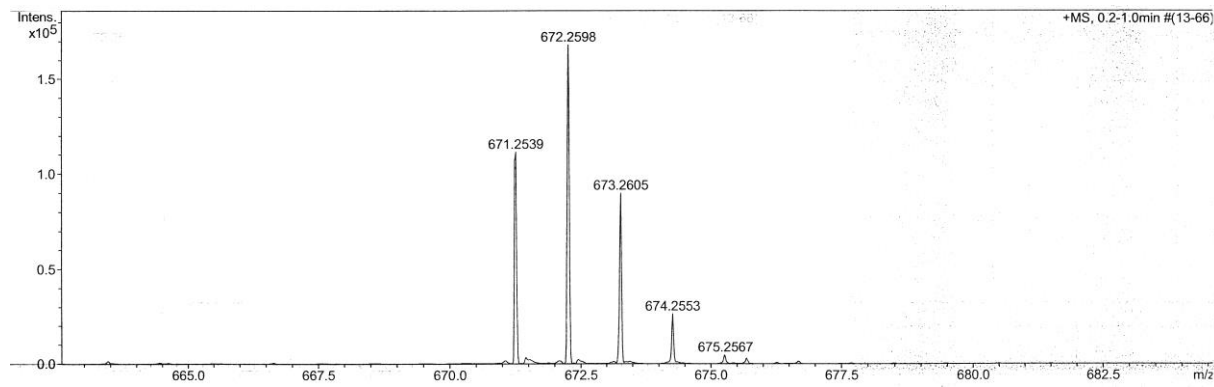


Figure S28. The HR-MS spectrum of *p*-Bpor (ESI+, TOF)

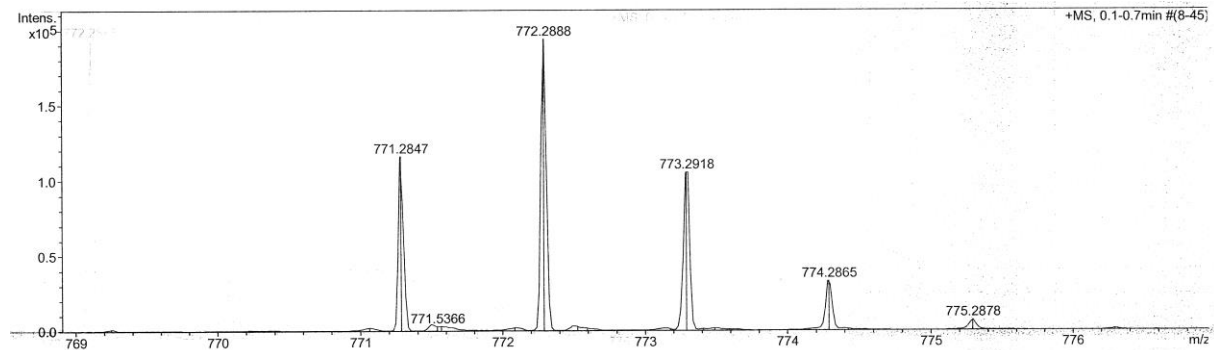


Figure S29. The HR-MS spectrum of Apor (ESI+, TOF)

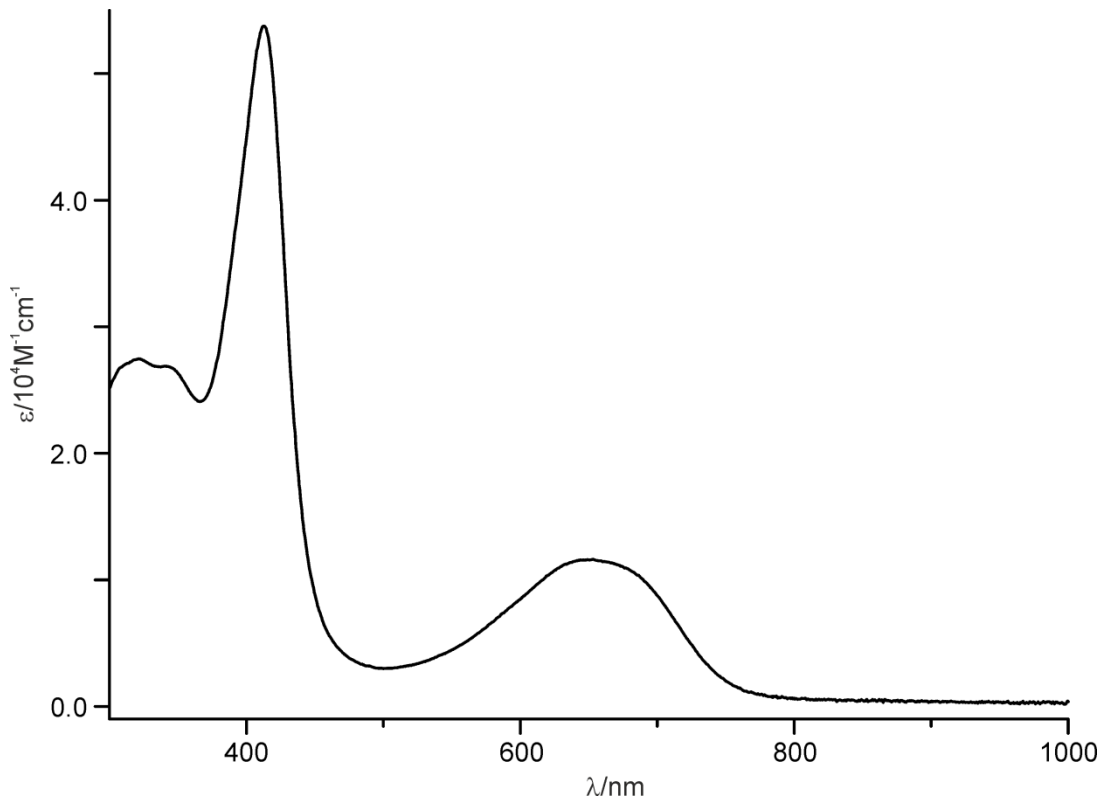


Figure S30. The electronic absorption spectrum of *m*-Bpor (dichloromethane, 298 K)

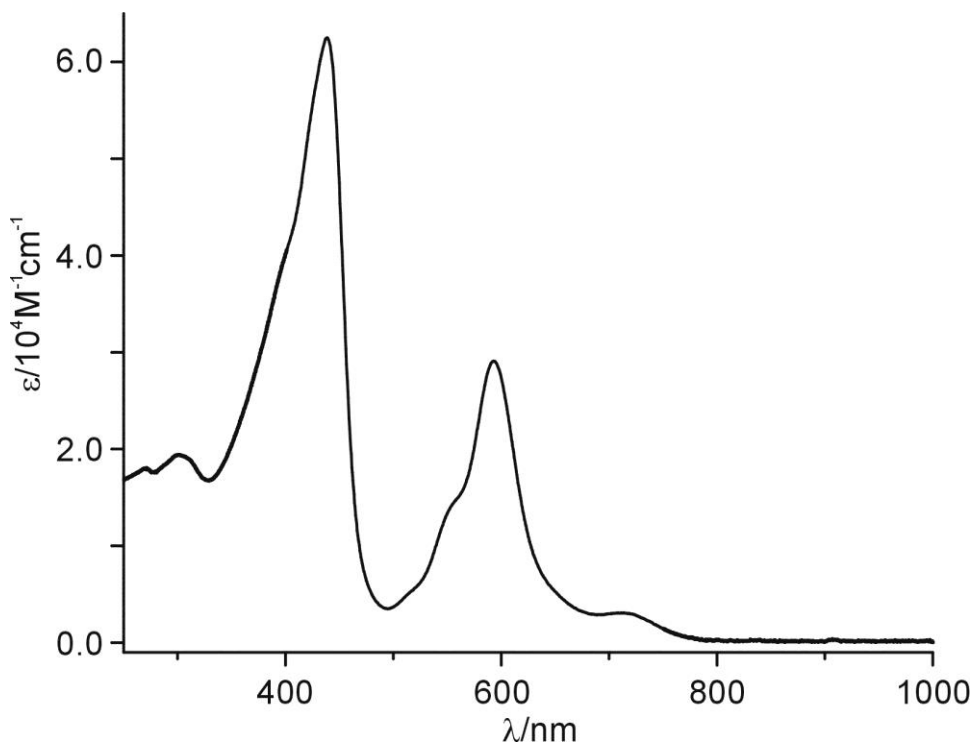


Figure S31. The electronic absorption spectrum of *p*-Bpor (dichloromethane, 298 K)

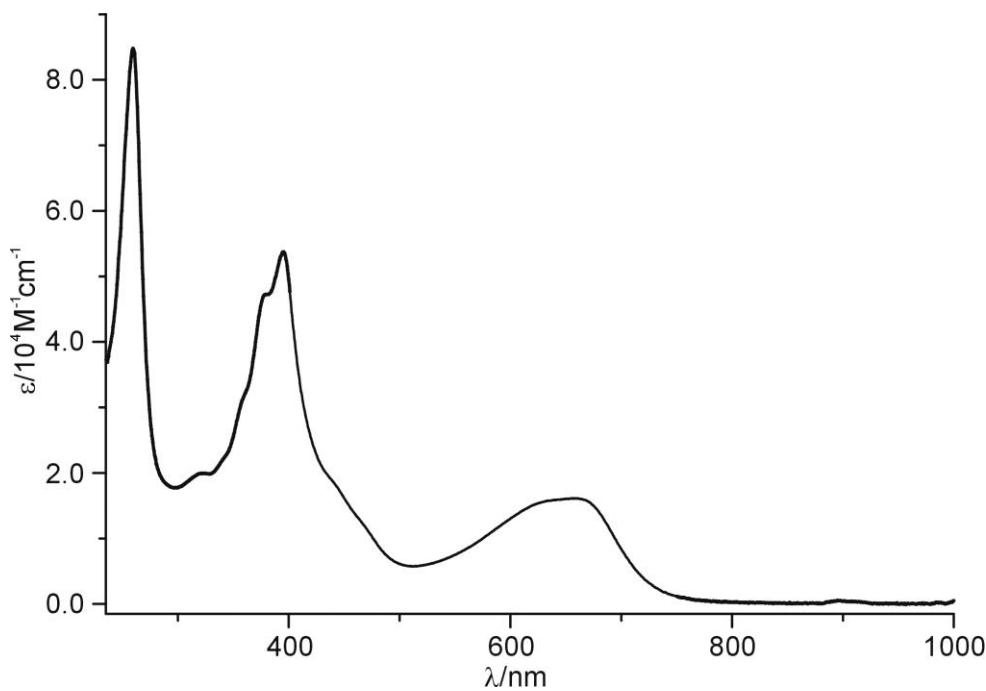


Figure S32. The electronic absorption spectrum of Apor (dichloromethane, 298 K)

Table S3. TD-DFT (B3LYP/6-31G(d,p)) calculated energies, oscillator strengths and compositions of the major electronic transitions of *m*-Bpor

Energy (cm ⁻¹)	Wavelength (nm)	Osc. Strength	Major contribs
13373.57	747.7434	0.2003	HOMO->LUMO (98%)
18607.34	537.4224	0.0493	H-1->LUMO (25%), HOMO->L+1 (74%)
22613.52	442.2133	0.0229	H-5->LUMO (24%), H-3->LUMO (26%), H-2->LUMO (44%)
23219.25	430.6771	0	H-5->LUMO (15%), H-3->LUMO (30%), H-2->LUMO (51%)
23770.94	420.6818	0.787	H-1->LUMO (66%), HOMO->L+1 (21%)
24558.95	407.1836	0.0392	H-5->LUMO (41%), H-3->LUMO (17%), HOMO->L+2 (37%)
24700.09	404.8568	0.1259	H-4->LUMO (84%)
25459.87	392.7749	0.0669	H-5->LUMO (12%), H-3->LUMO (16%), H-1->L+1 (29%), HOMO->L+2 (37%)
26084.15	383.3746	0.087	H-6->LUMO (75%)
26928.62	371.3521	0.0109	H-7->LUMO (89%)
27068.15	369.4378	0.0221	H-12->LUMO (35%), H-11->LUMO (15%), H-6->LUMO (16%), H-5->L+1 (10%), H-3->L+1 (12%)
28102.97	355.8343	0.3118	H-1->L+1 (57%), HOMO->L+2 (15%)
28671.59	348.7772	0.1676	H-10->LUMO (83%)
29391.05	340.2397	0.0012	H-8->LUMO (89%)
29393.47	340.2117	0.0061	H-9->LUMO (94%)
29678.18	336.9479	0.0362	H-2->L+1 (83%)
29827.4	335.2623	0.0079	H-11->LUMO (35%), H-5->L+1 (16%), H-3->L+1 (37%)
30058.88	332.6804	0.0016	H-12->LUMO (35%), H-11->LUMO (26%), HOMO->L+3 (26%)
30095.98	332.2703	0.008	H-4->L+1 (82%)
30612.98	326.6588	0.0275	H-13->LUMO (83%)
30629.12	326.4867	0.0624	H-12->LUMO (11%), H-11->LUMO (16%), HOMO->L+3 (67%)
31139.67	321.1338	0.0886	H-14->LUMO (15%), HOMO->L+4 (78%)
31493.75	317.5233	0.0385	H-14->LUMO (60%), HOMO->L+4 (12%)
31725.23	315.2065	0.0821	H-15->LUMO (70%), H-5->L+1 (13%)
32126.9	311.2657	0.1473	H-15->LUMO (10%), H-5->L+1 (35%), H-3->L+1

			(16%), H-1->L+2 (11%), HOMO->L+5 (16%)
32364.03	308.985	0.0007	HOMO->L+5 (65%)
32439.84	308.2629	0.0003	H-6->L+1 (78%)
32977.01	303.2415	0.0071	HOMO->L+6 (83%)
33160.1	301.5672	0.0135	HOMO->L+7 (69%), HOMO->L+9 (15%)
33227.85	300.9523	0.0001	HOMO->L+6 (11%), HOMO->L+8 (83%)

Table S4. TD-DFT (B3LYP/6-31G(d,p)) calculated energies, oscillator strengths and compositions of the major electronic transitions of *p*-Bpor

Energy (cm ⁻¹)	Wavelength (nm)	Osc. Strength	Major contribs
15773.89	633.9589	0.0887	H-1->LUMO (18%), HOMO->L+1 (81%)
16150.56	619.1737	0.325	H-1->L+1 (10%), HOMO->LUMO (90%)
23091.01	433.069	0.6116	H-1->LUMO (70%), HOMO->L+1 (14%)
23610.43	423.5416	0.0525	H-2->LUMO (82%)
24262.13	412.1649	0.3722	H-1->L+1 (69%), HOMO->L+2 (18%)
25104.18	398.34	0.0488	H-4->LUMO (32%), H-2->L+1 (49%)
25194.51	396.9118	0.068	H-4->L+1 (13%), H-3->LUMO (74%)
25829.28	387.1576	0.0885	H-5->LUMO (25%), H-4->L+1 (29%), HOMO->L+2 (23%)
25930.9	385.6402	0.0972	H-4->LUMO (57%), H-2->L+1 (24%)
26891.52	371.8645	0.1384	H-5->LUMO (13%), H-4->L+1 (49%), HOMO->L+2 (22%)
27112.51	368.8334	0.16	H-3->L+1 (75%)
27471.43	364.0145	0.026	H-7->LUMO (14%), H-5->LUMO (29%), H-3->LUMO (12%), HOMO->L+2 (20%)
27672.27	361.3726	0.1008	H-6->LUMO (87%)
28304.61	353.2993	0.0766	H-7->LUMO (66%), H-5->LUMO (19%)
28747.41	347.8574	0.0001	H-15->LUMO (12%), H-8->LUMO (56%)
29011.16	344.695	0.0003	H-11->LUMO (16%), H-9->LUMO (59%)
29216.02	342.2779	0.1874	H-8->LUMO (15%), H-5->L+1 (68%)
29337.01	340.8664	0.0046	H-8->L+1 (12%), H-6->L+1 (71%)
30157.28	331.5949	0.0015	H-8->L+1 (53%), H-6->L+1 (21%)
30429.9	328.6242	0.0689	H-9->L+1 (13%), H-7->L+1 (68%)
30884.8	323.7839	0.0079	H-11->LUMO (75%), H-9->LUMO (19%)
30932.38	323.2858	0.0032	H-10->LUMO (83%), HOMO->L+3 (11%)
31109.02	321.4502	0.0796	H-15->LUMO (27%), H-10->LUMO (12%), HOMO->L+3 (38%)

31201.77	320.4946	0.0081	H-11->L+1 (13%), H-9->L+1 (53%), H-7->L+1 (20%)
31667.16	315.7846	0.0097	H-14->LUMO (24%), H-13->L+1 (12%), H-12->LUMO (22%), HOMO->L+4 (37%)
31797.82	314.487	0.0099	H-13->LUMO (62%), HOMO->L+5 (10%)
32443.07	308.2322	0.0913	H-15->LUMO (44%), HOMO->L+3 (22%)
32495.5	307.735	0.0006	H-12->LUMO (52%), HOMO->L+4 (12%)
32528.56	307.4221	0.0492	H-1->L+2 (30%), HOMO->L+6 (42%)
32529.37	307.4145	0.0317	H-15->L+1 (21%), H-14->LUMO (15%), HOMO->L+4 (42%)

Table S5. TD-DFT (B3LYP/6-31G(d,p)) calculated energies, oscillator strengths and compositions of the major electronic transitions of Npor

Energy (cm ⁻¹)	Wavelength (nm)	Osc. Strength	Major contribs
15223.01	656.9002	0.2683	H-1->L+1 (10%), HOMO->LUMO (90%)
15610.97	640.5752	0.0308	H-1->LUMO (35%), HOMO->L+1 (64%)
19559.89	511.2504	0.3242	H-2->LUMO (11%), H-1->LUMO (59%), HOMO->L+1 (28%)
21695.66	460.9217	0.3154	H-1->L+1 (80%)
23370.88	427.8829	0	H-5->LUMO (16%), H-4->LUMO (21%), H-3->LUMO (54%)
24074.2	415.3824	0.2364	H-2->LUMO (78%)
24484.74	408.4176	0.0242	H-4->LUMO (67%), H-3->LUMO (26%)
25310.66	395.0905	0.1448	H-8->LUMO (11%), H-5->LUMO (44%), H-2->L+1 (19%)
25359.86	394.324	0.0037	H-10->LUMO (20%), H-6->LUMO (24%), H-5->L+1 (11%), H-4->L+1 (15%), H-3->L+1 (16%)
25628.44	390.1915	0.0001	H-2->L+1 (60%), HOMO->L+2 (27%)
26388.22	378.9569	0.0008	H-7->LUMO (12%), H-3->L+1 (12%), HOMO->L+3 (71%)
26447.91	378.1017	0.0808	H-9->LUMO (14%), H-8->LUMO (36%), HOMO->L+2 (33%)
26864.9	372.2329	0.0917	H-6->LUMO (55%), H-4->L+1 (12%), H-3->L+1 (15%)
27452.08	364.2712	0.1904	H-7->LUMO (32%), H-4->L+1 (10%), H-3->L+1 (17%), HOMO->L+3 (15%)
27552.09	362.9489	0.0682	H-8->LUMO (38%), H-5->LUMO (28%), HOMO->L+2 (15%)
27632.75	361.8895	0.0019	H-7->LUMO (41%), H-4->L+1 (34%), H-3->L+1 (20%)
27912.62	358.2609	0	H-9->LUMO (70%)
28460.28	351.3669	0.1512	H-10->LUMO (49%), H-6->LUMO (11%), H-4->L+1 (18%)
28803.06	347.1853	0.0189	H-10->L+1 (20%), H-7->L+1 (11%), H-6->L+1 (53%)
29160.37	342.9312	0.3494	H-10->LUMO (14%), H-8->L+1 (14%), H-5->L+1 (39%)

29812.88	335.4255	0.0088	H-7->L+1 (63%), H-6->L+1 (10%)
30009.68	333.2258	0.0335	H-9->L+1 (12%), H-8->L+1 (44%), H-5->L+1 (24%), H-1->L+2 (12%)
30291.97	330.1204	0.0202	H-11->LUMO (91%)
30416.18	328.7723	0.0253	H-12->LUMO (90%)
30622.66	326.5555	0.0145	H-1->L+2 (70%)
30746.87	325.2363	0.0092	H-10->L+1 (55%), H-6->L+1 (28%)
31106.6	321.4752	0.048	H-9->L+1 (62%), H-8->L+1 (30%)
31263.07	319.8662	0.0004	H-15->LUMO (36%), HOMO->L+4 (47%)
31509.88	317.3608	0.0148	H-14->LUMO (79%), HOMO->L+5 (11%)
31796.21	314.5029	0.0944	H-13->LUMO (45%), H-1->L+3 (27%), HOMO->L+4 (15%)

Table S6. TD-DFT (B3LYP/6-31G(d,p)) calculated energies, oscillator strengths and compositions of the major electronic transitions of Apor

Energy (cm ⁻¹)	Wavelength (nm)	Osc. Strength	Major contribs
13470.36	742.3707	0.0093	H-1->LUMO (97%)
13965.59	716.0458	0.2562	HOMO->LUMO (93%)
17873.37	559.4916	0.1412	H-2->LUMO (10%), HOMO->L+1 (84%)
18975.13	527.0056	0.1452	H-1->L+1 (90%)
21630.33	462.3139	0.0022	H-2->LUMO (10%), HOMO->L+2 (90%)
23069.23	433.4779	0.0031	H-8->LUMO (10%), H-6->LUMO (14%), H-4->LUMO (11%), H-3->LUMO (62%)
23570.91	424.2518	0.0093	H-4->LUMO (61%), H-3->LUMO (25%)
24153.25	414.023	0.2815	H-5->LUMO (43%), H-2->LUMO (41%)
24243.58	412.4803	0	H-8->LUMO (46%), H-6->LUMO (12%), H-4->LUMO (22%)
24866.24	402.1516	0.4782	H-5->LUMO (53%), H-2->LUMO (31%)
25017.88	399.7142	0.0542	H-6->LUMO (12%), H-1->L+2 (67%)
25462.29	392.7376	0.2085	H-8->LUMO (14%), H-6->LUMO (26%), H-1->L+2 (25%), HOMO->L+3 (29%)
25535.69	391.6088	0.0067	H-13->LUMO (16%), H-10->LUMO (20%), H-7->LUMO (43%)
26419.68	378.5057	0.0072	H-6->LUMO (13%), H-2->L+1 (36%), HOMO->L+3 (32%)
26582.6	376.1859	0.0466	H-10->LUMO (22%), H-7->LUMO (53%)
26722.14	374.2215	0.0411	H-9->LUMO (77%), H-6->LUMO (10%)

27282.7	366.5327	0.0044	H-1->L+3 (97%)
28188.47	354.755	0.0908	H-13->LUMO (25%), H-10->LUMO (38%), H-3->L+1 (11%)
28224.76	354.2988	0.0535	H-2->L+1 (47%), HOMO->L+3 (12%)
28356.23	352.6562	0.2162	H-10->LUMO (11%), H-3->L+1 (69%)
29107.94	343.5488	0.0051	H-11->LUMO (18%), H-5->L+1 (67%)
29245.06	341.9381	0.0427	H-4->L+1 (75%)
29375.72	340.4172	0.0052	H-11->LUMO (79%), H-5->L+1 (13%)
29482.19	339.1879	0.0226	H-13->LUMO (16%), H-12->LUMO (75%)
30107.27	332.1457	0.0026	H-13->LUMO (24%), H-8->L+1 (49%), H-4->L+1 (11%)
30520.23	327.6515	0.0011	H-15->LUMO (46%), H-14->LUMO (41%)
30664.6	326.1089	0.0009	H-16->LUMO (77%), H-8->L+1 (10%)
30886.41	323.767	0.0079	H-15->LUMO (28%), H-14->LUMO (27%), H-10->L+1 (15%)
31007.39	322.5037	0.1879	H-6->L+1 (57%), H-3->L+1 (10%)
31042.88	322.135	0.0321	H-10->L+1 (12%), H-7->L+1 (47%)